Title

INFRARED SPECTROSCOPY OF ADSORBATES ON METALS: DIRECT ABSORPTION AND EMISSION

Authors

Richards, P.L.
Tobin, R.G.

Publication Date

1985-09-01

Lawrence Berkeley Laboratory
UNIVERSITY OF CALIFORNIA

Materials & Molecular Research Division

To be published as a chapter in **VIBRATIONAL SPECTROSCOPY OF MOLECULES ON SURFACES**, Vol. 4 of **METHODS OF SURFACE CHARACTERIZATION**, J.T. Yates, Jr. and T.E. Madey, Eds., Plenum Publishing Corp., New York, NY

INFRARED SPECTROSCOPY OF ADSORBATES ON METALS: DIRECT ABSORPTION AND EMISSION

P.L. Richards and R.G. Tobin

September 1985

Prepared for the U.S. Department of Energy under Contract DE-AC03-76SF00098

DISCLAIMER

LBL-20228

INFRARED SPECTROSCOPY OF ADSORBATES ON METALS: DIRECT ABSORPTION AND EMISSION

P. L. Richards and R. G. Tobin

Department of Physics, University of California

and Materials and Molecular Research Division

Lawrence Berkeley Laboratory

Berkeley, California 94720

TABLE OF CONTENTS

I. Introduction

Measurements of the vibrational spectra of monolayers or sub-monolayers of adsorbates on surfaces present a severe challenge to the infrared spectroscopist. In many cases, multiple surfaces cannot be used and small signals must be measured that are superimposed on background radiation that can be many orders of magnitude stronger. To be successful, an experiment must be both well conceived and well executed. The conventional approaches are transmittance and reflection-absorption spectroscopy. Hoffmann[1] and Ryberg[2] have reviewed the reflection-absorption technique. Many approaches have been used to enhance the size of the surface signal relative to the backgrounds. These include multiple reflection,[3,4] attenuated total internal reflection,[5] surface electromagnetic waves,[6] and Stark modulation,[7] as well as direct measurements of absorption and emission. In this paper we will review some aspects of infrared technology that are relevant to this measurement problem and then describe direct absorption and emission techniques as applied to the vibrational spectroscopy of adsorbed atoms and molecules on metal surfaces. The techniques described will have applications to other surface spectroscopies such as atoms or molecules adsorbed on transparent insulators and to chemiluminescence, but the discussion will focus on the important, and especially difficult problem, of the vibrational spectroscopy of adsorbates on metals.

The high conductivity of metals insures that the infrared electric vector at the position of the adsorbate is very nearly perpendicular to the surface. The infrared beam must have a large angle of incidence to produce this perpendicular field. Under these conditions, 10-20% of the incident beam is absorbed in the metal and 80-90% is reflected. A very much smaller amount is absorbed in the adsorbed layer. The large metallic absorption arises from the fact that the penetration depth for photons in the metal is much larger than atomic or molecular dimensions. Measurement of the reflected beam appears to be the most straightforward way to obtain vibrational information for the adsorbate. This information, however, comes superimposed on a background that is 80-90% of the incident infrared beam. Variations in this background, whether due to source fluctuations, spectrometer instability, or photon statistics appear as noise.

The background encountered in a reflection absorption experiment is not fundamental. Techniques which measure the power absorbed in the sample, or the power emitted by the sample, have lower backgrounds by a factor of order 10 than reflection experiments. Since most carefully designed experiments are limited by the ability to cancel these backgrounds, this can be a worthwhile improvement. One quantity of interest is the ratio of the strength of the molecular signal to the signal absorbed by, or reflected by, the metal. In Fig. 1 (b) we show this ratio as a function of incident angle for CO chemisorbed on Ni. We see that the fractional molecular signal peaks at large angles of incidence for both absorption and reflection, but that the peak is both wider and higher for absorption than reflection. The advantage of

direct absorption measurements is even greater for metals with higher conductivity such as Cu, Ag, Au or Pt. Since interesting surface species are being studied which have peak absorptivities less than 10^{-4}, however, a background signal corresponding to an absorptivity of 10^{-1} or even 10^{-2} is far from negligible. For this reason it is in principle easier to measure a given small adsorbate signal on a lossless dielectric substrate than on a metal.

The large background encountered in any infrared experiment on a metal substrate requires careful attention to the modulation scheme used. Ideally, the modulation in an IR surface experiment serves two functions: to distinguish the surface signal from the substrate background, and to avoid low frequency noise and drifts. In general, a single modulation technique may not accomplish both objectives.

The surface signal can be isolated by comparing spectra measured with and without an adsorbate present. The drawback of this approach is that it represents a modulation on the time scale of minutes to hours; it is therefore very susceptible to low frequency drifts. A second form of faster modulation is generally needed in addition. Sensitivity to drifts is minimized if the fast modulation is also partially surface selective. Two modulation schemes that also distinguish surface from substrate contributions are polarization modulation[4,8,9] and wavelength modulation.[2,10,11]

Polarization modulation exploits the fact that only the p-polarized component of the infrared beam contains the surface signal. A rotating polarizer[4,8] or photoelastic modulator[9] switches the polarization of the beam. After demodulation, the detector signal is proportional to the difference in intensity between the two polarizations. When the spectrometer efficiency is strongly polarization-dependent as is typically the case with a grating instrument, a second polarizer, fixed at an angle between the s- and p-orientations, should be used after the switched polarizer. In principle, the fixed polarizer keeps the polarization state of the light entering the spectrometer fixed, regardless of the orientation of the switched polarizer. In practice, imperfections in available infrared polarizers limit the usefulness of this approach. Nonetheless, over selected frequency ranges,[8] or with a less polarized spectrometer,[9,12] polarization modulation can be used very effectively.

In the case of wavelength modulation,[10,11] the wavelength incident on the detector is modulated, giving a signal after demodulation proportional to the derivative of the intensity with wavelength. This approach enhances sharp spectral features over broad ones. It therefore emphasizes the adsorbate signal if it is sharper than other spectral features in the background. The infrared emissivity of metals is essentially featureless. The spectrometer efficiency, however, must have no sharp structure in the frequency range of interest. For such a system, wavelength modulation can be very useful.[10,11]

In the preceding discussion, it is tacitly assumed that background variations are the primary limit to sensitive surface measurements. We

believe that this is true for well designed experiments, but it is far from obvious. Traditionally, infrared spectroscopy has been source brightness or, nearly equivalently, detector noise limited. Developments in infrared technology have occurred, however, which make it possible to avoid detector noise in the types of experiments under discussion.

A difficult spectroscopic problem, such as the measurement of the vibrational properties of monolayers of adsorbates on metal surfaces, can benefit from the most careful experimental analysis. In order to make this analysis comprehensible, we will present in Section II a summary of the present status of some relevant techniques of infrared spectroscopy. In Section III we describe an experiment which measures the heat deposited in the metal substrate by the infrared flux from a blackbody source. This experiment is based on the technology of low temperature bolometric detectors developed for astronomy at submillimeter wavelengths. It provides high sensitivity and broad wavelength coverage, but is not easily compatible with the techniques used to produce clean single crystal surfaces. In this respect its limitations are similar to some of the acoustic detection techniques that are used with laser sources.[13]

In Section IV we describe an infrared emission experiment in a cooled environment which has been used to measure the vibrational frequencies of CO on clean, well characterized single crystal surfaces of Ni and Pt. This experiment is compared and contrasted with other emission experiments designed to measure monolayer adsorbates on metals.

Again, infrared technologies recently developed for astronomy can be used to optimize such measurements.

II. Status of relevant technology

A. Overview

For many years infrared spectra were measured in the vibrational frequency range from 400 to 4,000 cm^{-1} using thermal sources, diffraction grating spectrometers, and room temperature detectors. These techniques are convenient, and sensitive enough to do many important measurements. Spectroscopists who needed high resolution, or longer wavelengths, increasingly used cooled photon detectors and/or cooled bolometric detectors. Since ratios of signal-to-noise remained a problem, the prejudice arose that infrared spectroscopy is detector noise (or source brightness) limited.

Fourier transform infrared spectroscopy (FTIR) is being used increasingly. In addition to the multiplex advantage over dispersion spectrometers that is available when the spectroscopy is detector noise limited, Fourier Michelson spectrometers can have high resolution with relatively high throughput and can cover very wide spectral bands without changes in optical components. The computer necessary for Fourier analysis has proved very useful for co-adding spectra and accurate data manipulation, especially for applications such as surface spectroscopy in which large backgrounds must be subtracted. The factors which influence the choice of an infrared spectrometer will be discussed in more detail below.

Tunable laser sources suitable for vibrational spectroscopy have become increasingly available for near and middle infrared wavelengths.

These sources have been extraordinarily useful for very high resolution measurements, for nonlinear effects, and for short pulse measurements which require large power density in a narrow spectral band. They have also greatly expanded the usefulness of a variety of modulation and detection techniques for measuring weak absorptions.[13,14]

Lasers are of unquestioned value for surface Raman spectroscopy[15] and surface nonlinear spectroscopies,[16] which may prove very useful in the future. The role of laser sources in linear infrared spectroscopy of monolayer coverages of molecules on metal surfaces is not obvious. Because of the large background signals, sources are required that have very high amplitude stability. The spectral range of interesting molecular vibrations is wider than that covered by the more generally available tunable infrared lasers. Infrared free electron lasers now under development, however, promise a wider tuning range. If high stability can be maintained, then these new lasers may prove very useful for linear surface infrared spectroscopy. Since only moderate resolution is required, the narrow linewidth of infrared lasers is not a critical advantage. Useful reviews of the performance of tunable lasers are available.[17,18]

The power available from laser sources permits the use of relatively inefficient modulation or detection schemes which can in principle enhance the adsorbate signal relative to the background. A microphone[14] or a thermometer attached to the sample can measure the absorbed power, rather than the reflected power. As will be discussed in Section III below, however, the thermometric technique can also be used effectively with thermal sources. In either case, they are not

easy to make compatible with the cleaning procedures used to produce well characterized single crystal surfaces. This difficulty is avoided by a technique which detects the thermal distortion of the sample surface due to absorbed laser power.[13] Another technique uses an electric field to Stark shift the signal. This enhances the adsorbate signal relative to the metallic absorption.[7] The achievable frequency shifts are small compared to typical linewidths, but the approach is very promising when stable tunable lasers are available.

The synchrotron radiation from electron storage rings is widely used for UV and X-ray spectroscopy. There has been some interest in using the infrared output from such facilities. Calculations of the infrared radiation from storage ring sources show that they are considerably brighter than conventional laboratory thermal infrared sources. Unfortunately, however, the throughput available at most infrared wavelengths is considerably less than is used for most laboratory infrared spectroscopy. Consequently there is only a moderate improvement in useful infrared power, except for experiments that can only make use of very small throughput.

In order to characterize the image that can be formed from a storage ring source (or from any partially coherent source) it is useful to define a normalized throughput $A\Omega\nu^2$, where A is the area of a focal spot, Ω is the solid angle of convergence, and ν is the wavenumber. This quantity is variously called the phase space volume or the number of modes. The latter name arises from the fact that a diffraction-limited beam (with a single transverse mode) has

$A\Omega = \nu^{-2}$.[19] For a thermal source the power per mode in the wavenumber interval $d\nu$ is

$$p_\nu d\nu = hc^2\nu[\exp(hc\nu/kT) - 1]^{-1} d\nu \qquad (1)$$

for one polarization. In the Rayleigh-Jeans limit (1) reduces to the Johnson noise expression

$$p_\nu d\nu = kTcd\nu \; . \qquad (2)$$

Incoherent radiation, such as that typically obtained from a thermal source, can be described as consisting of a large number of these modes. The Planck spectral distribution, giving the spectral power into a throughput $A\Omega$, can be obtained from Eq.(1) by multiplying by the number of polarizations times the number of modes $P_\nu = 2A\Omega\nu^2 p_\nu$. It is convenient to describe the output of any source (thermal or non-thermal) in terms of distribution of modes and an effective Rayleigh Jeans temperature $T_{eff} = p_\nu/kc$, which is a measure of the power per mode. The effective temperature T_{eff} for a thermal source is equal to the physical temperature for $hc\nu \ll kT$ and falls exponentially for $hc\nu \gg kT$ as is shown in Fig. 2.

The effective temperature for a storage ring source with a tightly focused electron beam is proportional to the beam current and is essentially independent of frequency in the infrared. The value of T_{eff} calculated[20] for synchrotron radiation from a bending magnet of a proposed new storage ring, the Advanced Light Source, is compared with typical blackbody sources in Fig. 2. Calculations for existing storage

rings such as the National Synchrotron Light Source give a slightly higher T_{eff} at low infrared frequencies due to a larger beam current, but with some falloff at high frequencies due to the spread of the electron beam.[21] Also shown in Fig. 2 is the output expected from one type of magnetic wiggler introduced into a straight section of the ALS. Although such wigglers are very useful in increasing T_{eff} at higher frequencies, the type shown here is of limited value in the infrared. Interest in storage ring infrared sources arises from the fact that T_{eff} is 10^3-10^4 times higher than for thermal sources at infrared frequencies.

A complete comparison between thermal and storage ring sources, however, must include consideration of the available distribution of modes. A typical Fourier spectrometer designed for vibrational spectroscopy using a thermal source operates with an f/1 focus on a detector area of 1 mm^2. This corresponds to $A\Omega\nu^2 = 10^4$ modes at ν = 1000 cm^{-1} and 10^6 modes at ν = 10,000 cm^{-1}. The infrared beam from a bending magnet on a storage ring by contrast is fan shaped. It is diffraction limited (one mode high) in the vertical direction and has the full range of bend angles in the horizontal direction. If the same detection system is used, the number of available modes is only 10^2 at 1000 cm^{-1} and 10^3 at 10,000 cm^{-1}. Thus the total power from the storage ring in this application is about equal to that from a thermal source in the vibrational frequency range. It is substantially larger, however, at far infrared wavelengths.

The comparison is somewhat more favorable for the storage ring in the reflection absorption surface spectroscopy experiment. The narrow

range of angles shown in Fig. 1 over which a large fractional surface signal is obtained is well adapted to the fan shaped beam from the storage ring. About one order of magnitude more signal in the vibrational frequency range can be expected for such a source than for a thermal source.

In this review we will argue that when modern detectors are properly used, infrared spectroscopy of molecules on metal surfaces with thermal sources need not be source power or detector noise limited. Therefore only modest advantages can be expected from using a more powerful source, and then only if the source is stable and conveniently tunable. This argument for the usefulness of thermal sources is valid only if experiments are carefully optimized to minimize ambient photon noise.

The infrared spectral range coincides very closely with the spectral range over which the thermal emission from room temperature objects is important. The presence of this background thermal radiation has a profound influence on the design of many infrared experiments. This ambient photon flux can saturate sensitive detectors. Fluctuations in this flux very often dominate system noise. Sensitive experiments with visible light are usually done in a dark room so that the effects of ambient photons can be neglected. At longer wavelengths the brightness of the ambient thermal photons increases rapidly. In the far infrared, thermal sources are only a factor 3 brighter than room temperature. Conditions comparable to those achieved at visible wavelengths in a dark room can only be achieved by cooling the "room." One major advantage of bright sources such as lasers or even storage rings is that large ratios

of signal to noise can be obtained with less effort required to control the ambient thermal flux.

In this paper we will describe two infrared surface experiments that use thermal sources. The design of these experiments is dominated by the need to reduce ambient photon noise. A quantitative understanding of photon noise is essential for this task. Although the literature contains many descriptions of photon noise,[22] the equations are difficult to use correctly without some knowledge of how they arise. In the next section we present an overview of the subject of photon noise at infrared wavelengths.

B. Photon Noise

For our purposes we can distinguish three types of incoherent square law detectors. In photovoltaic detectors a fraction η of the incident photons above a cutoff wavenumber ν_c generates electron-hole pairs that migrate to the electrodes. The photocurrent that arises from a photon rate $\dot{N}$ (which is assumed to lie in the wavenumber interval between ν and $\nu + d\nu$) is $I = G\dot{N}e$. The noise in this photocurrent, in the ideal case, arises from fluctuations in the rate of arrival of infrared photons.

In extrinsic photoconductive detectors, a fraction η of the incident photons creates either mobile electrons or mobile holes, which move under the influence of an externally applied field. These carriers produce a photocurrent $I = G\eta\dot{N}e$. Here G is the photoconductive gain, which is equal to the ratio of the carrier lifetime to the transit time. It expresses how many times a mobile carrier can cross the detector before it is lost through recombination or trapping. The noise in this photocurrent, in the ideal case, arises both from fluctuations in the rate of arrival of incident photons (which controls the rate of generation of mobile carriers) and from the statistically independent rate of recombination which eliminates these carriers.

In thermal detectors a fraction η of the incident photons dissipate their energy as heat. The resulting temperature change is read out by a thermometer whose output is often a voltage. The output voltage is given by $\eta\dot{N}hc\nu S$, where S is the voltage responsivity in [V/W]. As will be discussed in Section III-b below, the fundamental noise in thermal detectors comes both from fluctuations in the rate of arriving photons, and from internal thermal fluctuations.

For photon detectors the absorptive quantum efficiency η is essentially zero for $\nu < \nu_c$ and is a slowly varying function of frequency with typical values from 0.1 to 0.5 for $\nu > \nu_c$. For thermal detectors η is called the absorptivity. It is typically a weak function of frequency and >0.5 for all important frequencies.

In order to understand photon noise we focus our attention on the number $\eta\dot{N}t$ of charge carriers generated in a photovoltaic detector in some arbitrary time interval t. Since these photons arrive at random

under the conditions of interest for this article, Poisson statistics can be used to compute the root-mean-square fluctuation in this number of charges $\Delta(\eta\dot{N}t)_{RMS} = (\eta\dot{N}t)^{1/2}$. The RMS output noise current averaged over time t is thus $\Delta(\eta\dot{N}t)_{RMS}\, e/t = e(\eta\dot{N}/t)^{1/2}$, where e is the electronic charge. Since the post-detection noise bandwidth associated with averaging over a time t = 0.5 s is one Hz, the noise current per unit post-detection bandwidth is $\Delta I_{RMS} = e(2\eta\dot{N})^{1/2}$ [A $Hz^{-1/2}$] for a photovoltaic detector, and $\Delta I_{RMS} = Ge(4\eta\dot{N})^{1/2}$ [A $Hz^{-1/2}$] for an extrinsic photoconductive detector. By considering the energy associated with photon fluctuations, photon noise in the output of a thermal detector can be written $\Delta V_{RMS} = hc\nu S(2\eta\dot{N})^{1/2}$ [V $Hz^{-1/2}$] if the detector is cold enough that its own radiation can be neglected.

It is traditional to define the noise-equivalent photon rate $NE\dot{N}$ as the photon rate that must be incident on a detector for the output current to be equal to the root mean square fluctuation per unit bandwidth in the output current. For a photovoltaic detector this condition is $\eta eNE\dot{N} = e(2\eta\dot{N})^{1/2}$. The resulting noise equivalent photon rate is

$$NE\dot{N} = \left(\frac{2\gamma\dot{N}}{\eta}\right)^{1/2} \quad [\text{Photons } s^{-1}\ Hz^{-1/2}]. \tag{3}$$

where $\gamma = 1$ for a photovoltaic and $\gamma = 2$ for a photoconductive detector. Similarly, we can define a noise equivalent power NEP as the incident signal power required to obtain an output signal equal to the RMS output noise. The result is

$$NEP = hc\nu\left(\frac{2\gamma\dot{N}}{\eta}\right)^{1/2} \quad [W\ Hz^{-1/2}], \tag{4}$$

where ν is the wavenumber of the photons. For a cold thermal detector $\gamma = 1$.

The photons that cause the fluctuations in detector output can be the signal from a thermal source with temperature T and emissivity ε that reach the detector through a spectrometer with throughput $A\Omega$ and transmittance τ. Alternatively they may come from the room, or the spectrometer itself. The Planck theory gives the power spectrum $P_\nu d\nu$ (or photon rate $\dot{N}_\nu\, d\nu$) that reaches the detector in the throughput $A\Omega$ and the wavenumber range from ν to $\nu + d\nu$,

$$\dot{N}_\nu d\nu = \varepsilon\tau\, A\Omega_{eff}\, B(\nu,T)\, d\nu/hc\nu, \tag{5}$$

where $B(\nu,T) = 2hc^2\nu^3(\exp hc\nu/kT - 1)^{-1}$.

To be precise, $\Omega_{eff} = \int_\Omega \cos\theta d\Omega$ where θ is the angle between the propagation direction and the normal to the radiating surface.

If photons are incident on the detector over a significant fractional bandwidth, then the mean square fluctuations arising from photons at different frequencies must be added in the appropriate way. For a photon detector, the fraction η of the incident photons at any frequency above the cutoff creates essentially equivalent mobile carriers. A relatively simple expression can be obtained if we assume that η is independent of frequency over the band of interest. For a photovoltaic detector,

$$\Delta I_{RMS} = e\left[2\eta \int_{\nu_c}^{\infty} \dot{N}_\nu d\nu\right]^{1/2} \quad [A\ Hz^{-1/2}]. \tag{6}$$

If we use $\dot{N}_\nu$ from Eq. (5) then for either type of photon detector

$$N\dot{E}N = \left| \frac{4\gamma A\Omega_{eff} k^3 T^3}{\eta c^2 h^3} \int_{x_c}^{\infty} \frac{\varepsilon\tau x^2 dx}{e^x - 1} \right|^{1/2}, \tag{7}$$

where $x = hc\nu/kT$. We assume that the infrared band is defined by the frequency dependence of the product $\varepsilon\tau$ of emissivity times transmittance which includes the effects of filters and spectrometers. This noise equivalent photon rate is the most convenient quantity for evaluating the performance of photon detectors. Unfortunately the practice has arisen of converting $N\dot{E}N$ to $NEP = N\dot{E}N\ hc\ \langle\nu\rangle$ where $\langle\nu\rangle$ is a weighted average infrared frequency,

$$\langle\nu\rangle = \int_{\nu_c}^{\infty} \varepsilon\tau \dot{N}_\nu \nu d\nu \Big/ \int_{\nu_c}^{\infty} \varepsilon\tau \dot{N}_\nu d\nu \tag{8}$$

This tradition is harmless for narrow infrared bands, but introduces unnecessary complexity when broad bands are involved.

For thermal detectors such as bolometers, the absorptivity η is approximately constant in frequency, but the energy per photon is proportional to frequency. Thus the power fluctuations which arise from photons at different frequencies are weighted properly by summing the mean square voltage fluctuations in the detector output

$$\Delta V_{RMS} = \left[2\eta \int_0^\infty \dot{N}_\nu \, \nu^2 \, d\nu\right]^{1/2} hcS, \tag{9}$$

so that

$$NEP = \left| \frac{4A\Omega_{eff} k^5 T^5}{\eta c^2 h^3} \int_0^\infty \frac{\varepsilon\tau x^4 dx}{e^x - 1} \right|^{1/2} \quad [W\ Hz^{-1/2}]. \tag{10}$$

We now have a complete prescription for calculating the minimum noise to be expected from a detector that is subjected to a known infrared flux. Under certain practical situations, where the detector responsivity and quantum efficiency (or absorptivity) are known from the manufacturer, the values of $\dot{N}$ or p_ν can be deduced from the electrical output of the detector. The expected photon noise can then be computed from Eqs.(3) and (4) [or (7) and (10)] and compared with the measured noise. This is one practical way in which the question of whether the detector is photon noise limited under its operating conditions can be answered.

Another approach to estimating photon noise is to compute the incident power from the temperature and the geometry of the infrared sources. As an example consider a source temperature $T = 10^3$ °K and a spectrometer throughput $A\Omega = 10^{-2}$ srcm^2, efficiency (or transmittance) $\tau = 0.1$, and wavenumber bandwidth $\Delta\nu$, which can be broad for an FTS or narrow for a dispersion spectrometer. Signal photon fluctuations are very important at visible, or higher frequencies, where there are few energetic photons, but don't usually limit infrared measurements. Using the above numbers for $\Delta\nu = 1$ cm^{-1} at $\nu = 10^3$ cm^{-1} gives a signal power $p_\nu d\nu = 3.7 \times 10^{-7}$ W and a signal photon limited NEP $= 6 \times 10^{-14}$[WHz$^{-1/2}$] for a ratio of signal-to-noise S/N $= 6 \times 10^6$ [Hz$^{-1/2}$].

As an example of background photon noise consider 300°K background radiation incident through a 2π solid angle ($\Omega_{eff} = \pi$) at all frequencies above the detector cutoff on an ideal photon detector with $\eta = 1$. This ideal photon detector limit[22] depends on the detector cutoff frequency. It varies from NEP $= 8 \times 10^{-12}(A)^{1/2}$[W Hz$^{-1/2}$] for a detector which cuts off at $\nu_c = 2000$ cm^{-1}, has a maximum value of $3.8 \times 10^{-11}(A)^{1/2}$ for $\nu_c = 800$ cm^{-1} and falls to $1 \times 10^{-11}(A)^{1/2}$ at 100 cm^{-1}. It is known as the background limited infrared photoconductor (BLIP) limit. It is important to note that this so called limit can be avoided by reducing the background temperature or by reducing the solid angle or bandwidth with cooled optical components.

When 300°K radiation is incident at all frequencies on an ideal cooled thermal detector with absorptivity $\eta = 1$, the NEP obtained from Eq. (7) is $4\times10^{-11}(A)^{1/2}$[W Hz$^{-1/2}$] where A is the detector area in [cm^2]. The minimum noise in a room temperature thermal detector is larger than this value because fluctuations in the emitted photons must also be included. Since photon noise and several other sources of noise vary as $A^{1/2}$, detector performance is sometimes specified in terms of the specific detectivity $D^* = A^{1/2}/NEP$[W^{-1}Hz$^{1/2}$ cm].(22)

C. Detectors

Modern photoconductive detectors operated at low temperatures have noise very close to that given by the photon noise limit in Eq.(1) with $\eta \gtrsim 0.1$ for a wide range of values of the incident photon rate N. An example of this performance is given(23) in Fig. 3. When used with conventional amplifiers(24) these detectors become amplifier noise limited at photon rates $\lesssim 10^7$ photons/sec, corresponding to NEP = 2×10^{-17} W Hz$^{-1/2}$ at 10 μm. Specialized amplifiers exist, however, with noise levels which become important only below ~100 photons/sec.(25) Some of these detectors are listed in Table 1.

These high performance detectors have been developed for the exacting requirements of space infrared astronomy with cooled optics.(26) For nearly all laboratory experiments the background photon rate is so large that a much wider variety of cooled detectors,

TABLE 1. PROPERTIES OF SOME HIGH PERFORMANCE PHOTOCONDUCTIVE DETECTORS.

Detector Material	Cutoff Wavenumber (cm^{-1})	Cutoff Wavelength (μm)
Si:In	1,400	7
Si:Bi	625	16
Si:As	370	27
Ge:Be	175	57
Ge:Ga	83	120
Stressed Ge:Ga	50	200

can approach the background photon noise limit, including nearly all of the well known photovoltaic detectors such as InSb, HgCdTe, and PbSnTe. These photovoltaic detectors typically have higher operating temperatures and are thus often more convenient to use than the extrinsic photoconductive detectors listed in Table 1. Since most infrared detectors are sold for applications in which they view a large amount of 300°K background, it is sometimes difficult to obtain specifications or test results relevant to low background applications.

Several types of photoconductive and photovoltaic infrared detectors are becoming available in integrated arrays of tens to thousands of detectors. The readout is accomplished by methods related to those used with the Si CCD arrays which are sensitive to visible frequencies.

The most sensitive available thermal detectors are semiconductor bolometers.(27) In low backgrounds such bolometers have NEP's approaching $10^{-15}[WHz^{-1/2}]$ when operated at liquid ^{4}He temperatures, and at least one order of magnitude better at lower temperatures.(28) Photon noise limited operation can be achieved in almost any imaginable surface experiment. A detailed discussion of bolometric detectors will be given in Sec. III.

An infrared experiment can be optimized by cooling apertures and filters (or spectrometers) to minimize the background photon rate. and then selecting a detector and amplifier system good enough to be limited by the fluctuations in the detected photons coming both from the background and from the source.

D. Spectrometers

The most frequently used infrared spectrometers are the Fourier Michelson spectrometer, often referred to as the Fourier transform spectrometer or FTS, the grating spectrometer, and the Fabry-Perot spectrometer. The FTS has the well known multiplex advantage. If the noise in the system remains constant as the bandwidth over which the signal power falls on the detector is changed, as is the case for inherent detector noise, then the FTS can measure the entire spectrum of n spectral elements in essentially the same time that a grating or Fabry-Perot spectrometer with similar efficiency and throughput takes to obtain a single spectral element with the same signal-to-noise ratio.

The multiplex advantage of Fourier spectroscopy is often used successfully to reduce the effects of the noise from a relatively insensitive, but convenient, room temperature detector such as the pyroelectric detector. It is a common experience that the substitution of a more sensitive cooled detector does not achieve the anticipated degree of improvement. This can occur because the noise is no longer independent of the bandwidth over which signal power falls on the detector.

As we have seen, detectors exist for which detector noise is negligible for nearly all laboratory experiments. When a photon noise limited detector is used, noise varies as the square root of the signal power as the bandwidth is changed, and there is no multiplex advantage. The performance of a single frequency spectrometer is nearly equivalent to that of a multiplexed spectrometer for such optimized experiments. A third case exists in which the noise is proportional to the signal power falling on the detector. Such noise could arise from fluctuations in

the source, microphonics in the optics, chopper noise, etc. In this case the Fourier spectrometer has a multiplex disadvantage and takes n-times longer to measure the spectrum than the narrow band spectrometer. As with other types of noise, only that portion of the source noise spectrum that is close to the modulation frequency is important. A rapid scan FTS does not have a multiplex disadvantage for slow drifts in source intensity. Such slow drifts are important, however, in any surface experiment that requires the subtraction of spectra taken many minutes apart.

Diffraction grating spectrometers can be used with a linear array of n detectors in the dispersed output. This gives a multichannel advantage of a factor n in time, whatever the source of noise. As high quality integrated arrays become available with $n \geq 10^2$, the grating spectrometer will often be the device of choice for optimized experiments at moderate resolution, particularly since it is much easier to cool than the Fourier spectrometer.

The FTS and the Fabry-Perot spectrometer can give higher throughput at high resolution than the grating spectrometer.[29] For the relatively low resolution of ~1 cm^{-1} needed for vibrational spectroscopy of chemisorbed molecules and the limited throughput available with samples at grazing incidence, this difference is often not of great importance.

The FTS is very convenient to use, compared with grating or Fabry-Perot spectrometers, when a wide spectral band is to be covered. It is thus the practical choice for many spectroscopic problems that do

not have to be carefully optimized. For difficult problems such as measurements of the vibrational spectra of molecules chemisorbed on metal surfaces, alternative spectrometers should be considered.

E. Conclusions for surface spectroscopy

From this discussion of infrared techniques, it should be clear that there are a number of alternative approaches to the problem of infrared surface spectroscopy. The required throughput, resolution, spectral range, and ratio of signal to detector or photon noise can be obtained in several ways. The most critical aspect of a measurement of vibrational spectra on metals, however, arises because small signals must be observed that are superimposed on large backgrounds. This aspect of the measurement imposes additional requirements which are very demanding. First, the experiment should be designed to minimize these backgrounds. Second, a background subtraction scheme must be implemented and third, all parts of the experiment should be extremely stable on the time scale of the background subtraction.

In the following sections of this paper we describe two experiments in which the background is minimized by measuring the sample absorptivity and emissivity, rather than the reflectivity. This is done with some sacrifice in signal level. In both cases, however, the experiments have been optimized so that detector and photon noise do not play an important role. The surface sensitivity achieved is limited by the precision with which the remaining background has been subtracted.

III. Direct Absorption Spectroscopy

A. Techniques for measurement of absorbed power.

Direct absorption spectroscopy requires some method of detecting a change in the sample caused by the absorption of infrared power by the adsorbed molecules. The most straightforward method, and the one used in the experiments described here, is simply to measure the rise in sample temperature due to the absorbed power using a sensitive thermometer thermally coupled to the sample. In this method the sample itself is used as a bolometric infrared detector.

There are other techniques used to detect absorbed power which involve the generation of sound in the sample, or the thermal expansion of the surface. Typical sensitivities of such techniques are on the order of 10^{-8} W $Hz^{-1/2}$ or worse,[13] which is many orders of magnitude worse than bolometric detection. This sensitivity is not sufficient for use with thermal or storage ring sources. As stable tunable lasers become available over the spectral band of interest for vibrational spectroscopy, these techniques will become more important.

B. Sensitivity of Thermal Detection

In the direct absorption measurement described here, a thermometer attached to the metal sample serves as the detector of absorbed infrared power. The structure used is very similar to that of the composite far infrared bolometer,[27,28] which has been brought to a high state of development for use in infrared astronomy. The infrared flux in the surface experiment is very large compared with that encountered in the astronomy experiments, so many of the stringent design requirements for

those detectors can be relaxed. Before discussing optimization of the surface experiment in detail, it is useful to review the simple theories of bolometer response and noise.

We consider a bolometer whose electrical resistance R(T) is a known function of its temperature T. The bolometer is assumed to have heat capacity C and to be connected to a heat sink at temperature T_S by a thermal conductance G. Since the absorbed infrared power is partly chopped or interference modulated, it is written $P = P_0 + P_1 e^{i\omega t}$. The bolometer temperature then varies as $T = T_0 + T_1 e^{i\omega t}$. By equating the infrared and electrical power dissipated in the bolometer with the power conducted to the heat sink and stored in the heat capacity we have the linearized equation,

$$P_0 + P_1 e^{i\omega t} + I^2 R(T_0) + I^2 \frac{dR}{dT} T_1 e^{i\omega t} = G(T_0 + T_1 e^{i\omega t} - T_S) + i\omega C T_1 e^{i\omega t} . \quad (11)$$

The steady state part of Eq. (11)

$$P_0 + I^2 R(T_0) = G(T_0 - T_S), \quad (12)$$

gives the value of G required to keep the bolometer cold. The time varying part of Eq.(11) can be solved for the temperature responsivity T_1/P_1. A more useful quantity is the voltage responsivity $S = V_1/P_1 = IT_1(dR/dT)/P_1$ which gives the voltage response of a bolometer that is biased with a constant current I,

$$S = \frac{I(dR/dT)}{[G - I^2(dR/dT)] + i\omega C} = \frac{I\alpha R}{G_{eff}(1 + i\omega\tau_{eff})} . \quad (13)$$

We have followed the conventional practice by defining an effective thermal conductance $G_{eff} = G - I^2(dR/dT)$ and an effective time constant $\tau_{eff} = C/G_{eff}$. The temperature dependence R(T) is characterized by the parameter $\alpha = (dR/dT)/R$ evaluated at $T = T_o$. The most useful thermometers for composite bolometers or surface absorption experiments are made from heavily doped and compensated semiconductors, eg. Si or Ge, which conduct by hopping of carriers between impurity sites. This process[30] gives $R(T) = R_H \exp[(T_H/T)^{1/2}]$ so that $\alpha = -1/2(T_H/T^3)^{1/2}$. The proper choice of thermometer parameters is desirable to minimize certain noise mechanisms. If the bolometer bias current is obtained from a constant voltage source and a load resistance $R_L > R$, which is cooled to T_S, then noise from the bias circuit can be made negligible.[31] The most important sources of noise are then the photon noise discussed in Section II, the Johnson noise from the bolometer resistance R, and the thermal fluctuation noise from the thermal conductance G.

In order to compare the magnitudes of these noise contributions, it is conventional to express each one as an NEP referred to the bolometer input. The photon noise is given in this form in Eq.(10). The mean square voltage spectral density for Johnson noise is 4kTR per unit bandwidth. The resulting contribution to the NEP for unit bandwidth is

$$NEP_J = \left(\frac{4kTR}{|S|^2}\right)^{1/2} \quad [WHz^{-1/2}] \; . \tag{14}$$

Energy fluctuations, which occur whenever an object, such as a bolometer, with heat capacity C is connected to a heat sink through a thermal conductance G, can be computed by conventional thermodynamic arguments.(32) The thermometer attached to the bolometer will read a mean square temperature fluctuation $\langle(\Delta T)^2\rangle = kT^2/C$. This total fluctuation can be written as an integral over a temperature spectral density of the form $\langle(\Delta T)^2\rangle_\omega = 4kT^2/G_{eff}(1 + \omega^2\tau^2_{eff})$. The frequency dependence comes from that of $|S|^2$ in Eq.(10). Then if $\omega\tau_{eff} << 1$, the temperature spectral density is $4\ kT^2/G_{eff}$ per unit bandwidth. Converting to a power fluctuation at the detector input we obtain,

$$NEP_T = (4\ kT^2G_{eff})^{1/2}\ [W\ Hz^{-1/2}]. \tag{15}$$

Since NEP is a measure of a signal-to-noise ratio and since the frequency dependence of S enters in both the signal and the noise, Eq.(15) is valid for all frequencies.

In direct absorption measurements on surfaces it may be inconvenient to reduce C until $\omega\tau_{eff} << 1$. If experiments are done with $\omega\tau_{eff} > 1$ then the responsivity S is reduced. This in turn increases the NEP due to Johnson noise and amplifier noise. There is no penalty in sensitivity until one of these noise sources becomes comparable with the photon noise.

Since photon, Johnson and thermal contributions to the noise are statistically independent, the observed NEP[31] is the square root of the sum-of-the-squares of the contributions in Eqs. (10), (14), and (15).

For a surface absorption experiment using a thermal source and a rapid scan FTS the throughput is limited by the sample to $A\Omega \simeq 10^{-2}$ sr cm^2 and the optical bandwidth can be thousands of cm^{-1}. For ideal performance, the steady state infrared power P_0 should not be much larger than the modulated power P_1, and the bolometer should be photon noise limited. In practice it is difficult to reduce the ambient background to this value in a UHV system. Excess ambient background power P_0 increases the photon noise and requires a larger G to keep the bolometer cold. This in turn increases NEP_T. It also reduces the responsivity S which increases NEP_J. It is thus of highest importance to use cooled baffles, filters and apertures to keep the throughput and spectral bandwidth for P_0 nearly equal to those for P_1.

The arguments sketched above show that even if there is no source noise, the noise in a system that has been properly optimized for a given spectral bandwidth will generally increase as the spectral bandwidth is increased. Under these conditions a multiplex advantage cannot be expected from the FTS. A multiplex disadvantage might even arise. Cooled filters can then be used with profit to limit the spectral bandwidth. There is often a tradeoff between the convenience of a wide spectral range and the possibility of a higher signal-to-noise ratio with a narrow range.

C. The direct absorption instrument

In this section, we will describe an instrument for direct absorption spectroscopy developed at Berkeley by Bailey, et al.(33) This description will include the spectrometer, the optical system, the UHV chamber, and the sample configuration. We will then compare the observed performance of the system with that estimated from the detector parameters. Even though the detector achieves photon noise limited performance, the surface experiment is limited--as in most surface infrared experiments--by other instabilities that affect the background subtraction. Nevertheless, the instrument is capable of detecting as little as 10^{-3} L of CO on an evaporated silver film.

The spectrometer used in this experiment is an EOCOM 7001P rapid scan FTS. It has a spectral range of 400-4000 cm^{-1}, with a maximum resolution of 0.065 cm^{-1}. Although the instrument is purged continuously with dry air, small amounts of water vapor always remain. The change in the water absorption with time can easily dominate the surface signal when spectra taken hours apart must be compared. Thus the system has so far been used primarily at frequencies greater than 1800 cm^{-1}, where water vapor absorption is small. This limitation can be overcome with the use of an evacuated spectrometer, and such a modification is planned.

The infrared beam from the spectrometer enters the vacuum chamber through an indium-sealed KRS-5 window. It is then focused onto the sample by a KRS-5 lens located inside the vacuum chamber. At the sample, the beam has a half-angle of 9.1°, and is incident at an angle of 83° to the surface normal. The system throughput, for a 4 x 8 mm sample, is then $A\Omega = 3.1 \times 10^{-3}$ sr cm^2. The power absorbed by the sample from the spectrometer beam is typically 16 μW.

The minimum mirror speed of the spectrometer is 0.07 cm s^{-1} corresponding to a modulation frequency of 280 Hz for an infrared frequency of 2000 cm^{-1}. This property of the spectrometer is an important constraint on the detector design, giving $\omega\tau_{eff} = 1$ at $\tau_{eff} = 0.6$ ms.

As we have already discussed, the FTS offers little fundamental advantage over a dispersion instrument, since neither the multiplex advantage nor the throughput advantage is significant. It is, however, a stable and convenient instrument with a rapid modulation frequency.

In this direct absorption experiment, the sample is part of a bolometric infrared detector. The requirements of low heat capacity and sensitive thermometry impose severe constraints on the operating temperature and the type of sample that can be measured. In order to obtain adequate response time and detection sensitivity a heat sink temperature $T_S \sim 1.2°K$ was used. The samples were evaporated metal films deposited on a dielectric substrate (sapphire) which has a high Debye temperature and high thermal conductivity at low temperature. From the point of view of heat capacity, most crystalline dielectric or semiconducting substrates could be used. It would be very desirable to be able to use single crystal metal substrates. Because of the large heat capacity of metals at liquid helium temperatures, however, metal thicknesses would have to be $\lesssim 0.1$ mm. Such samples are difficult, but not impossible, to produce by grinding [34] or by epitaxial growth.[35,36] A second obstacle to the use of single crystal samples is the high annealing temperatures traditionally used while cleaning the sample. The thermometer technology used at present involves epoxy and/or indium solder, so it is limited to temperatures below 150°C. A

technique for heat sinking the thermometer during annealing has been developed which was successful but inconvenient.[33] Other techniques emphasizing higher temperature materials seem possible, but have not been demonstrated.

The decision to use evaporated film substrates greatly simplifies the vacuum system, though at some cost in sample characterization. Since a new film can be deposited at the beginning of each experiment, elaborate facilities for cleaning and characterizing the surface are not required. Moreoever, true ultrahigh vacuum conditions are needed only while the experiment is actually in progress. At these times a cold finger at ~1.2°K must extend into the chamber, so cryopumping by the liquid helium temperature surfaces can be used to reduce the pressure in the vicinity of the sample. At other times, a base pressure of 10^{-9} torr or even higher is adequate.

Based on these considerations, the design shown in Fig. 4 was chosen. The primary vacuum chamber is pumped by a 15 cm cryotrapped diffusion pump. A separate vacuum chamber surrounds the containers for liquid nitrogen and liquid helium. A cold finger, which is an extension of the liquid helium tank reaches into the UHV chamber and terminates in a copper plate, to which the sample assembly is attached. The sample is surrounded with a radiation shield, also at liquid helium temperature. There are several holes in the radiation shield, providing access to the sample from the outside. A liquid nitrogen-cooled radiation shield, with holes aligned with those in the helium-cooled shield, surrounds the cold finger. Between the two shields is a rotatable shutter at liquid nitrogen temperature, which selects only certain directions of access to the sample, depending upon its position.

This elaborate system of shielding is necessary in order to minimize the amount of room temperature radiation reaching the sample during the infrared measurement, yet provide access to the sample as needed for film deposition and dosing with adsorbate molecules. With the shields fully closed to minimize incident radiation, only 1.8 μW of background loading is absorbed in the sample, much less than the power from the spectrometer. Because of the effective shielding, it is not practical to dose the sample by filling the chamber with gas. Instead, an effusive beam doser with direct line-of-sight to the sample is used.

It should be noted that the need for such cold shielding makes the use of standard surface analysis tools such as LEED and Auger spectroscopy difficult. A two-level system, with an unshielded level for surface analysis and preparation at relatively high temperature, and a shielded level for the infrared measurement would be useful for measurements of well characterized samples.

The detector configuration chosen is a composite design developed for infrared astronomy,[27,28] which is easily adapted for a wide range of infrared power levels. A drawing of the bolometer is shown in Fig. 5. The front surface of the sapphire substrate is coated with 50 Å of Cr followed by 1000 Å of Au; this metallic coating insures good adhesion of the sample metal films that are subsequently deposited. The thermometer is a small, (~1 mm), cube of neutron transmutation doped Ge with ion-implanted ohmic contacts.[28,30] It is attached to the substrate with a small quantity of thermally conductive epoxy.[37]

Copper leads, 0.005 cm in diameter, are attached to the chip with indium solder. A thermocouple consisting of 0.005 cm diameter copper and constantan wires is also glued to the back of the substrate. The thermocouple is used to monitor the temperature when the sample is deliberately heated above a few degrees kelvin. At low temperatures, the thermal conductivity of alloys such as constantan is negligible compared to that of pure, non-superconducting metals such as copper, so the three copper leads provide the dominant thermal conductance, G, between the bolometer and its heat sink. Tungsten wires are used both to support and to heat the sample.

The measured properties of the bolometer, under operating conditions are given in Table II. It can be seen that the calculated and measured dc responsivities are in close agreement. The time constant gives $\omega\tau_{eff} \approx 15$ at 300 Hz, so that $|S|$ is reduced by a factor 15 from its dc value. Since Johnson noise and amplifier noise are still negligible, this roll-off in responsivity does not reduce the sensitivity.

The measured noise spectrum of the detector circuit is dominated by large peaks at the harmonics of 60 Hz. The mirror speed of the interferometer is chosen so that the resulting peaks in the infrared spectra do not interfere with the spectral range of interest. Between the peaks, a white noise level of 75 nV $Hz^{-1/2}$ is observed at a modulation frequency of 300 Hz. This level corresponds to an NEP of 1.9×10^{-12} W $Hz^{-1/2}$, in excellent agreement with the value estimated from the known properties of the bolometer and the infrared loading. Evidently the detector system approaches photon noise limited performance.

TABLE II. Typical operating conditions for the sample in the direct absorption experiment, including both calculated and directly measured values for responsitivity and noise from Eqs.(4) and (10-12)

Sink temperature	$T_S = 1.2°K$
Bolometer temperature	$T_o = 1.8°K$
Electrical resistance	$R = 3.3\ M\Omega$
Bias current	$I = 0.5\ \mu A$
Temperature coefficient	$\alpha = 2.2°K^{-1}$
Thermal conductance	$G = 3\times10^{-5}\ W°K^{-1}$
Effective thermal conductance	$G_{eff} = 3.2 \times 10^{-5}\ W°K^{-1}$
Time constant	$\tau_{eff} = 7.9\ ms$
Heat capacity	$C = 2.2\times10^{-8} J°K^{-1}$
Calculated dc responsivity	$S_C = 7.5\times10^{5} VW^{-1}$
Measured dc responsivity	$S_M = 5.8\times10^{5}\ VW^{-1}$
Absorbed photon power	$P_o = 16\ \mu W$
Average frequency	$\nu = 10^{3}\ cm^{-1}$

Contributions to the NEP at 300 Hz:

Calculated photon noise	$NEP_P = 8.0\times10^{-13}\ W\ Hz^{-1/2}$
Calculated Johnson noise	$NEP_J = 4.7\times10^{-13}\ W\ Hz^{-1/2}$
Calculated thermal noise	$NEP_T = 7.6\times10^{-14}\ W\ Hz^{-1/2}$
Calculated total noise	$NEP = 9.3\times10^{-13}\ W\ Hz^{-1/2}$
Measured noise voltage	$\Delta V_{RMS} = 75\ nV\ Hz^{-1/2}$
Measured NEP = $\Delta V_{RMS}/S_M$(300 Hz)	$= 1.9\times10^{-12}\ W\ Hz^{-1/2}$

We will see, however, that the ultimate sensitivity of the surface spectroscopy experiment is limited at a higher level by other effects. It is, of course, for precisely this reason that the direct absorption and emission techniques are attractive, since the substrate signal to be subtracted is much lower than in reflection-absorption spectroscopy.

We can use the known NEP of the detector, and the spectrum of the absorbed power, to estimate the sensitivity of the system to a small spectral feature on the smooth background of the substrate absorption. The power absorbed in a silver substrate in a 4 cm^{-1} bandwidth at ν = 2000 cm^{-1} has been measured to be approximately 2.3×10^{-8} W. Based on the known NEP, we calculate that the system should have a sensitivity to fractional changes in the absorptance of 8.3×10^{-5} $Hz^{-1/2}$. That is, in a one Hz bandwidth, the system should be able to detect a surface feature with an absorptance less than 10^{-4} of the substrate absorptance, with a signal-to-noise ratio of unity.

In Fig. 6, we show the spectrum of 10^{-3} L of CO on an evaporated silver film. A spectrum of the clean film has been subtracted, and the result divided by the reference. An additive constant is included for clarity of display. The total integration time for the spectrum was approximately 2400 s. The integrated intensity of the CO signal, expressed as a fraction of the bulk absorptance, is 8.3×10^{-4}, and the noise level, in the same terms, is 1.7×10^{-4}, corresponding to a sensitivity of 1.2×10^{-2} $Hz^{-1/2}$. This sensitivity is some 150 times worse than that calculated from Table II. Clearly, as is usually the case with surface infrared experiments, it is not the detector sensitivity but errors in the cancellation of the background, that limit

the ultimate sensitivity of the measurement. Nevertheless, Fig. 6 clearly illustrates that the direct absorption technique is capable of detecting extremely small quantities of adsorbates, and very weak vibrational signals.

D. Experimental results: CO on Ag

As an example of the use of infrared absorption spectroscopy, we summarize here some results for CO adsorption on evaporated silver films. These data were obtained by Dumas, et al.,[38] using the apparatus described in the preceding section. They form part of an extensive investigation of CO adsorption on noble metal films. The complete results will be published elsewhere.[38,39]

We will discuss the three aspects of CO adsorption on evaporated silver: the dependence of the adsorption behavior on the temperature T_D of the sapphire substrate during the deposition of the silver film, the shift of the CO stretch frequency with coverage, and the integrated intensity of the CO stretch band.

It is found that the nature of the adsorption of CO depends strongly on T_D. For $T_D < 150°K$, only physisorbed CO can be detected when the sample is exposed to CO at 2°K. Fig. 7 shows a sequence of infrared spectra, as a function of CO exposure, in Langmuir, (L), for a film deposited at $T_D = 300°K$, which is well above the threshold temperature. The frequency of the single band, 2143 cm^{-1}, is equal to that for gas phase CO. This frequency, and the lack of any frequency shift with increasing coverage, are characteristic of physisorption. This result is consistent with the known behavior of CO on single crystal silver surfaces, which also do not support CO chemisorption.[40]

For a silver deposition temperature T_D = 4°K, which is well below the threshold temperature, the spectra, shown in Fig. 8, are quite different. At low coverages, a single band due to chemisorbed CO is observed. The band appears initially at 2148 cm^{-1}, and shifts to lower frequency as the coverage increases. The band reaches its full intensity at an exposure of 0.4 L. Evidently the film deposited at low temperature contains special active sites at which CO chemisorbs, in a concentration corresponding to ~40% of a monolayer on a single crystal. For exposures greater than 0.4 L, a sharp peak at 2143 cm^{-1}, due to physisorbed CO, appears in the spectrum. This physisorbed peak can be removed by heating to 25 K, while the band due to chemisorbed CO persists up to 80 K.

The shift of the vibrational band with exposure is also of considerable interest. Shifts of the band to higher frequency with increasing coverage are commonly observed for CO on transition metals.[41,42] This shift is attributed to the combined effects of a dynamic dipole-dipole interaction and a static, chemical interaction between neighboring molecules, mediated by the metal. For CO on Cu single crystals, the latter effect is known to cause a shift to lower frequency, with the result that the two effects very nearly cancel, resulting in little or no net shift.[10]

In the present case, for CO chemisorbed on a silver film deposited at low temperature, a large shift, (26 cm^{-1}), to lower frequency is

observed. The static and dynamic contributions to the shift can be separated by coadsorbing different isotopes. Because the isotopes have different resonant frequencies, they have negligible dynamic dipolar interaction.[43] However, the static chemical shift should be unaffected by the different mass of the neighboring coadsorbed molecules. Thus the observed shift is attributed entirely to the static effect, and the difference between the shifts observed in the two experiments can be assigned to the dynamic interaction. Fig. 9 summarizes the results of such a measurement. At low coverage, the chemical contribution fully explains the shift. At higher coverage, there is a difference between the total shift and the chemical shift, which is attributed to the dynamic interaction.

By means of coadsorption experiments with physisorbed CO and argon, it is found that a large part of the chemical shift occurs even when the coadsorbing molecules do not interact chemically with the surface at all. This effect is attributed to the influence of the local work function on the bonding of the chemisorbed molecule. A detailed discussion of this effect appears in the complete paper.[38]

The dynamic coupling is very well modeled by dipole-dipole coupling, including image effects as described by Persson and Ryberg,[44] with no need to invoke any additional dynamic coupling through the metal.[45] Fig. 10 shows the dynamic shift, as deduced from Fig. 9, and the integrated intensity of the chemisorption band, as a function of

coverage. The lines are a fit to the data using the dipole coupling theory, with the vibrational polarizability $\alpha_v = 0.27 \pm 0.015$ Å^3 and interaction potential $\tilde{U}(0) = 0.04 \pm 0.002$ Å^{-3}. Again, we refer the reader to the full paper for a detailed discussion.(38)

One of the reasons for investigating adsorption on noble metals deposited at low substrate temperature is that such systems are known to exhibit large enhancements in Raman cross section over the values observed either in the gas phase, or for adsorption on smooth single crystals.(15) This phenomenon is known as surface-enhanced Raman scattering, (SERS). A large part of the enhancement associated specifically with rough evaporated films has been attributed to electromagnetic resonances at visible frequencies.(15) It has also been suggested, however, that such films contain special Raman-active sites, not present on annealed films or single crystals, at which dynamic charge transfer greatly increases the Raman cross section.(15) It would be expected that molecules adsorbed at such sites, if they exist, would also exhibit much greater infrared absorption than commonly observed for adsorbed molecules. It has already been shown that rough silver films contain special chemically active sites, not present in annealed films, at which CO chemisorbs. It is interesting to inquire whether these might also be the postulated Raman-active sites, by comparing the infrared absorption by chemisorbed CO on rough silver films with that observed for CO on single crystals.

The polarizability α_v, used in the dynamic coupling model, allows such a comparison to be made. For a given fractional coverage of CO, the integrated intensity of the infrared absorption band is simply proportional to α_v. The value 0.27 $Å^3$ found for CO on evaporated silver is identical to that previously measured for CO on Cu(100).[10] There is thus no unusual enhancement of the infrared cross section associated with the special chemisorption sites found on the rough silver film, and no evidence for the hypothetical Raman-active sites.

E. Surface calorimetry

The sample design described here is optimized for the detection of small temperature changes caused by the dissipation of extremely small quantities of power in the sample. In the experiments discussed so far, the source of this power has been infrared radiation, and the purpose has been to measure the vibrational spectrum of the adsorbate layer. Such a sample configuration, however, is also ideally suited for the measurement of surface thermodynamic quantities at low temperature--that is, a bolometer is also an excellent differential calorimeter. In this section, we will discuss how the detector technology described here can be used for the measurement of various surface thermodynamic quantities.

Perhaps the easiest measurement of an important thermodynamic quantity that can be made with such an instrument is the direct determination of the binding energy of an adsorbate as a function of coverage. Normally, this quantity is measured indirectly, by thermal desorption spectroscopy, which generally requires additional assumptions about the kinetics of desorption.

When a molecule chemisorbs, virtually all of its binding energy is dissipated in the substrate as heat. If a flux of N molecules per second is incident on the sample from an effusive beam doser, or a molecular beam, and each molecule has a binding energy $E_b \sim 1$ eV, then the power deposited in the sample is $P = NE_b$. The kinetic energy of molecules from a 300°K source is $\sim 10^{-4}$ eV. For the detector we have described, the NEP at low frequencies and in the absence of infrared loading from the spectrometer is of order 8×10^{-14} W $Hz^{-1/2}$. For a particle rate of $N = 10^{10}$ s^{-1}, the sensitivity to changes in E_b is then 5×10^{-5} eV $Hz^{-1/2}$. In practice the accuracy of the measurement would certainly be limited by other uncertainties, predominantly in the determination of the molecular flux N. Geraghty et al.[46] have used a configuration similar to the one described here to measure the heat of adsorption of pyridine on Ni at 8°K.

Another thermodynamic measurement that can be performed with a bolometric detector is that of the heat capacity due to an adsorbate. Such measurements are particularly important in the study of surface phase transitions. In such an experiment, the infrared loading on the sample would be minimized, and a calibrated ac power applied by Joule heating of an auxiliary heater attached to the sample. The frequency chosen should be above $1/\tau_{eff}$, so that the response of the bolometer is dominated by the heat capacity C, rather than by the thermal conductance, G. The change in the sample heat capacity due to the

addition of an adsorbate will appear as a change in the amplitude of the temperature oscillation induced by the applied power.

This experiment can be approximately analyzed with the model used in Sec. III B, which includes an applied power of the form $P_0 + P_1(1 + e^{i\omega t})$. At a sufficiently high modulation frequency, temperature fluctuations become negligible, and the noise is limited by Johnson noise in the thermometer. In this limit, the minimum detectable change δC in the heat capacity is given by:

$$\left(\frac{\delta C}{C}\right)^2 = 4k \left(\frac{T_0}{T_1^2}\right) \frac{1}{I^2 R \alpha^2} , \qquad (16)$$

where the parameters are as defined in Sec. III B.

For the bolometer described above, the noise equivalent δC is 1.1×10^{-14} J°K^{-1}Hz$^{-1/2}$ at 1.8°K, and 2.2×10^{-12} J°K^{-1}Hz$^{-1/2}$ at 4°K, for $T_1 = 0.01$°K. The rapid decrease in sensitivity with increasing temperature is due primarily to the T^3 dependence of C and the exponential temperature variation of R. For comparison, the heat capacity of a layer of 10^{14} molecules, in a two-dimensional Debye model with a surface Debye temperature of 100°K, is 2.7×10^{-11} J °K^{-1} at 1.8°K, and 1.3×10^{-10} J °K^{-1} at 4°K, varying as T^2. From these estimates, it is clear that the bolometer should be able to detect the adsorbate contribution to the heat capacity rather easily. By carefully optimizing the detector and the operating parameters for heat capacity measurements in a particular temperature range, it should be possible to achieve even greater sensitivity.

IV. Infrared Emission Spectroscopy

A. The emission spectrometer

In this section we will describe a specific instrument for emission spectroscopy, indicating how the concepts and technologies discussed in the preceding sections influenced the design. A less tutorial description has been published elsewhere.[47]

The idea of using infrared emission spectroscopy for the study of surface vibrational modes is not new, but experiments using room temperature spectrometers have been plagued by low sensitivity. Griffiths[48] has reviewed work prior to 1975 on multilayer films on flat metal surfaces. A similar application has been the study of oxide growth on copper[49] and molybdenum[50] surfaces. Another approach has been to investigate monolayer adsorption on high surface area dispersed catalysts.[51-54] Blanke and Overend[4] proposed enhancing the sensitivity of the technique for flat surfaces by using a multiple reflection geometry, and demonstrated improved signal-to-noise ratio in the spectrum of a nine-layer Langmuir-Blodgett film. All of these experiments used room temperature spectrometers, with sample temperatures ~400-500°K. Allara, et al.[55] used a liquid nitrogen cooled FTS to obtain monolayer sensitivity on a flat metal surface at 300°K.

The goal of the instrument described here was to extend greatly the capabilities of infrared emission spectroscopy as a tool for surface science. It is the first system capable of measuring emission signals

from submonolayer coverages of adsorbates on clean, well characterized, single crystal metal substrates, over the frequency range from 400 - 3000 cm^{-1}, with moderate, (<10 cm^{-1}), resolution. The useful sample temperatures depend on the frequency chosen but are typically $\geq 250°K$. The most important factors affecting the design of the instrument were the small ratio, (10^{-4} - 10^{-2}), of the adsorbate emission to the substrate emission, and the availability of photoconductive detectors for the frequencies of interest that can approach the signal photon noise limit for the emission signal from the substrate alone. The first consideration required careful attention to modulation techniques and to system stability. The second motivated a major effort to minimize the amount of background radiation incident on the detector.

At 400 cm^{-1}, the photon fluxes from blackbodies at 300°K, 100°K, and 5°K are in the ratio 10^{59} to 10^{57} to 1. At higher frequencies the ratios increase exponentially. From these numbers it is clear that if the contribution to the radiation reaching the detector from the spectrometer is to be kept small compared to that from the sample at ~300°K (which is also the source), then all optical elements should be cooled at least to liquid nitrogen temperature. Since the Si:Sb photoconductive detector chosen required liquid helium cooling in any case, it was decided to cool the entire spectrometer to ~5K. In this way, drifts due to spectrometer emission were kept negligible compared with the small adsorbate signals. It is possible, however, to do

surface IR emission work, especially at higher infrared frequencies, with a liquid nitrogen cooled instrument.[55]

A diffraction grating spectrometer was chosen over an FTS system for several reasons. Since the detection is photon noise limited, no multiplex advantage was expected for an FTS. A multiplex disadvantage was possible. Since the throughput is sample limited, little throughput advantage could be realized from the FTS. The grating spectrometer was easier to cool. As will be discussed later, the possibility exists of using arrays of detectors in the dispersed output of the grating spectrometer to achieve a multichannel advantage. The optical layout of the emission system is shown in Figure 11.

The sample is maintained in an ultrahigh vacuum environment. An indium-sealed KRS-5 lens acts both as a vacuum window and as a focusing element, collecting the emitted radiation from the sample and focusing it on the entrance slit of the spectrometer. The lens is not cooled, but its emissivity is very low in the frequency range of interest. Nevertheless, variations in the small amount of radiation it emits can be a significant source of drift. Since the reflectivity of KRS-5 is ~40%, careful LN_2-cooled shielding has been used to minimize the reflection of radiation from warm objects into the beam. Even so, residual reflected radiation can cause slow drifts in the detector output. The effects of such drifts can be minimized by proper modulation of the signal.

The spectrometer is a compact Czerny-Turner design consisting of a planar steering mirror, off-axis paraboloidal collimator and camera mirrors, and a rotatable diffraction grating on an aluminum substrate. Six different gratings are used to cover the full spectral range with adequate resolution and efficiency, but the spectrometer must be opened to change gratings. All of the optical elements are bolted to a 30 cm diameter aluminum plate, which is screwed to the cold plate of a modified commercial liquid helium cryostat. Radiation shields at helium and nitrogen temperatures surround the spectrometer. Because of the large mass that must be cooled, it requires about two hours and eight liters of liquid helium to cool the spectrometer initially; thereafter, two liters of helium every twelve hours is sufficient to keep the system cold.

A filter wheel that can be rotated from outside the cryostat is located behind the entrance slit. Because of the low sample temperature, high orders of diffraction are eliminated by the exponential rolloff of the blackbody spectrum, so the usual low pass filters are not required. High pass filters are necessary, however, for measurements at frequencies well above the peak of the blackbody emission from the sample to avoid scattered low frequency radiation. A 2 mm thickness of LiF or MgF_2 is used for measurements above 1500 cm^{-1}. Another aperture of the filter wheel carries a polystyrene film for

frequency calibration. Frequency calibration can also be checked by observing the high order diffraction lines of He:Ne laser light directed on the sample through a window in the UHV sample chamber. The frequencies of many of the absorption bands in polystyrene do not appear to shift significantly with temperature.

An infrared polarizer is located on the LN_2 cooled shield of the spectrometer in front of the entrance slit. It is used to reject the s-polarized light from the sample which contains no adsorbate contribution.

The heart of the spectroscopic system is the detector. It is an extrinsic Si:Sb photoconductor sensitive to frequencies greater than 330 cm^{-1}, mounted in an integrating cavity to maximize quantum efficiency and provided with two apertures to minimize stray radiation. The cavity aperture gives a slit width of 1 mm and a system throughput of 2.5×10^{-3} sr cm^2. This should be compared with the maximum useful throughput of 2.5×10^{-2} sr cm^2 available from our 15 × 5 mm samples in the angular range from 65° to 85°.

The photon rate at the detector is in the range $\dot{N} = 10^9$ to 10^{10} photons s^{-1}. We use a conventional transimpedance amplifier[24] with a feedback resistor in the range 10^9-10^{10} Ω. This resistor is cooled to 5°K to reduce Johnson noise. The first stage of the amplifier is a commercial[56] dual JFET package heat sunk to the 5°K cold plate. The noise in this detection system is dominated by photon fluctuations for $\dot{N} > 10^8$ photons s^{-1}, at modulation frequencies above 10 Hz. At lower frequencies, system instabilities introduce additional noise and drift.

In order to perform any emission experiment, it is necessary to observe the sample against a background at a different temperature. To reduce background loading on the detector and to minimize the effect of instabilities, that background should be much colder than the sample. In our experiment this is achieved by including a liquid nitrogen cooled stage in the UHV chamber. Attached to the stage are shields to prevent stray ambient radiation from entering the beam, and a cold blackbody behind the sample, which prevents ambient radiation from reflecting off the sample into the spectrometer. The shields located in the UHV system are coated with gold black,[57,58] the reflectivity of which has been measured to be $< 1\%$ for $\nu > 500$ cm^{-1}. The emission spectrum of the gold black shows that it is well heat sunk to the underlying metal.

The emission system is sufficiently stable, even on the long time scale involved in the comparison of spectra with and without adsorbed molecules, that vibrational spectra can be obtained in a dc mode,[47] without the additional fast modulation discussed in Sec. I. More consistent baseline subtraction is achieved, however, when the emitted radiation from the sample is chopped. The chopper consists of a metal vane coated with gold black attached to a torsion bar, and driven to oscillate at its resonant frequency of 20 Hz by magnetic coils, giving a 40 Hz optical modulation. This chopper is essentially a UHV-compatible version of a commercial oscillating vane chopper.[59] It is mounted on the cold stage, so that the vane is cooled by conduction to -100°K. When the vane passes in front of the sample, the spectrometer looks at a cold, black surface.

Leakage signals past shields and emission signals from inadequately cooled objects in the optical train can contribute to the photon noise and, more important, can give signals which drift with time. Locating the chopper as close as possible to the sample insures that many such signals are not chopped, and so do not contribute slow drifts to the measurement. The chopper cannot discriminate against drifts in the temperatures of the sample and the cold stage, or of ambient radiation leaking around the input shield. The sample temperature is regulated to within 0.04°K using a thermocouple sensor spot-welded to the back of the sample. Better regulation would be desirable and could be obtained by using an infrared sensor. The cold stage temperature is maintained at ~100°K with a continuous flow of LN_2. Cooling it below 50°K with a mechanical refrigerator would eliminate this source of drift. It is difficult to completely prevent ambient temperature radiation inside the UHV system from entering the optical path. The cooled shield must have openings so that the sample can be moved into position for LEED and other surface characterization experiments.

Since the temperatures of the sample and the cold stage reference are very different, the measurement is sensitive to drifts in system gain. Two sources of gain drift have required attention. The amplitude of the chopped signal depends on the chopper drive amplitude, which must be adjusted to minimize sensitivity to amplitude fluctuations. Also, the amplifier gain depends on the temperature of the load resistor[24] through its temperature coefficient of resistance. This effect can be minimized by selecting load resistors. An alternative solution to the

gain drift problem is to use a reference source at or near the sample temperature. It should be black to avoid structure on its emission spectrum and small, to give a signal comparable to that of the sample. This approach has not been attempted.

If we assume that photon noise limits the sensitivity of the instrument, we can calculate the detection threshold for small molecular signals on a large background from the substrate. Figure 12[47] shows the result of such a calculation, assuming a substrate of emissivity 0.1 and a temperature of 300°K and using measured values of the spectrometer efficiency and detector quantum efficiency. The three solid lines, corresponding to three different gratings, indicate the minimum adsorbate signal (expressed as a fraction of the substrate emission) that could be measured with a signal-to-noise ratio of unity in a one Hz bandwidth. These lines represent the theoretical limit to the performance of the instrument if all extraneous noise sources were eliminated.

The dots shown in the figure represent the expected fractional signal due to a saturation coverage of various adsorbates on Pt(111). The values were estimated from published electron energy loss (EELS) spectra, using Ibach's[60] comparison of IR and EELS cross sections. The X's show our measured signal levels for the two observable modes of CO on Ni(100); these measurements will be discussed in more detail below. The *'s show the measured signal levels for CO on Pt(111). The strength of the technique, especially at the lower frequencies, where the vibrational modes tend to be weak, is immediately apparent.

In practice the photon noise limit has not been reached. The dashed lines show the measured sensitivity of the apparatus. The excess noise is limited by fluctuations in the stray radiation that enters the spectrometer despite the cold baffles. Since this source is modulated along with the sample emission, it is not greatly reduced by chopping. The chopper does, however, make it possible to achieve this level of performance quite consistently; in the dc mode, extra drifts often make the signal to noise ratio much worse. If the noise due to stray radiation were eliminated, the next limiting factor would probably be the stability of the source temperature.

B. Experimental results: CO on Ni(100)

The infrared emission apparatus has been used to measure both the intramolecular carbon-oxygen stretching vibration of CO on Ni(100),[61] (Fig. 13), and the low frequency molecule-substrate vibration for the same system,[62] (Fig. 14). Measurements of the molecule-substrate vibration of CO on Pt are in progress.[63] The observed linewidth of the C-Ni mode, 15 cm^{-1}, is in excellent agreement with the theoretical value of 13.9 cm^{-1}, which was subsequently calculated by Ariyasu et al.,[64] from the assumption that vibrational energy decay into substrate phonons dominates the linewidth. If this explanation of the linewidth is correct, then measurements of such adsorbate-substrate mode linewidths may be a very useful probe of energy transfer processes at surfaces. An attempt to verify the line-broadening mechanism by measuring the temperature dependence of the linewidth is still in progress. To date, only the infrared emission technique has been successful in measuring

the linewidths of such weak, low frequency vibrational modes as the C-Ni stretch. Other surface infrared spectroscopies have been limited to frequencies above ~1000 cm^{-1}.

In the case of the C=O stretch vibration data of Fig. 13, the observed linewidth is certainly not lifetime dominated. In fact, the narrowest lines, at very low coverage and at saturation, are not resolved at an instrumental resolution of 18 cm^{-1}. (A factor two better resolution, combined with higher efficiency, is now available with a new grating for this frequency range.) The lineshape is nonetheless interesting, for two reasons. First, the linewidth at saturation is a factor of two smaller than previously reported for this system.[65] This fact, combined with the absence of any band due to bridge-bonded CO--in agreement with LEED data[66] and recent electron energy loss spectroscopy results,[67] but in contrast to other published vibrational data[68,69]--leads us to believe that our surface was cleaner than in some other experiments. We found that even minute amounts (a few percent of a monolayer) of contamination gave rise to line-broadening and the appearance of bridging CO.

The second interesting feature is the shape of the inhomogeneously broadened bands at intermediate coverages. The band appears to consist of two unresolved lines. Neither the resolution nor the sensitivity of the experiment was adequate for a conclusive interpretation, but we have suggested an explanation in terms of island formation at low coverages.[61]

Both the possibly homogeneous linewidth of the C-Ni mode and the inhomogeneously broadened C=O mode need, and are receiving, further investigation. The data of Figures 13 and 14, however, are sufficient to demonstrate the power of infrared emission spectroscopy. The extension of high resolution spectroscopy to the weak vibrational modes in the frequency range of a few hundred cm^{-1} is a special feature of this instrument. The possibility exists of extending the frequency range still further, into the range of substrate phonon frequencies. The modifications necessary, while significant, appear possible.

C. Arrays and the multichannel advantage

In the spectrometer described here, a single detector is used, and a spectrum is measured by rotating the grating, sweeping the dispersed radiation across the detector. In principle, one could instead place a linear array of n detectors in the focal plane, and measure a range of frequencies simultaneously. Such a multichannel system has an $n^{1/2}$ advantage in signal-to-noise ratio over a single-detector instrument. In addition, the grating need not be moved, so that problems of the reproducibility of the grating position, and the generation of mechanical noise by the grating drive, are eliminated.

Arrays of ~10 discrete detectors are commonly used in infrared astronomy. Recently, however, monolithic arrays of large numbers of photoconductive detectors, (N = 10-1000), have appeared.[70] These detectors use technology developed for visible light detector arrays, and do not need the cumbersome individual amplifiers of discrete arrays. Because the detectors are arrayed on a single chip, high packing

densities, (~100 cm^{-1}), can be achieved. It can be expected that in the next few years, such detector arrays will become available for laboratory use, opening the possibility of large gains in sensitivity for infrared surface spectroscopy.

The exploitation of these detector arrays will require a spectrometer with a different optical design. The short focal length off-axis design of the spectrometer we have described here is very compact, but off-axis aberrations make it unsuitable for use with large arrays. As the size of the instrument is increased, the difficulties of cooling it increase as well. Such spectrometers have been successfully built and operated, however, for astronomical measurements.[71]

D. Non-Equilibrium Emission and Chemiluminescence

The discussion to this point has concerned the use of emission spectroscopy to observe the thermal equilibrium emission from adsorbed molecules. For this application, emission spectroscopy has an advantage over the more conventional technique of reflection-absorption spectroscopy only in its lower background. There is another class of experiments, however, for which emission spectroscopy is uniquely suited; these are experiments involving the detection of non-equilibrium radiation from excited species. Such an experiment has been carried out by Chuang[72] in the near infrared (1250-4000 cm^{-1}) region. The excitation mechanism was the chemical reaction of XeF_2 gas with a Si surface. The large amounts of energy released in this extremely fast, exothermic reaction resulted in intense chemiluminescence. With the

more sophisticated spectroscopic technology described here, much weaker signals could potentially be detected with higher spectral resolution opening an area rich in interesting phenomena.

As an example, consider an adsorbed molecule that has been electronically excited by a laser or a chemical reaction. In its electronic excited state, the equilibrium internuclear distance is perturbed, so that an electronic transition into the ground state is likely to leave the molecule vibrationally excited, via the familiar Franck-Condon effect. If infrared emission is emitted as the molecule then relaxes vibrationally, this radiation could potentially be detected with a cooled spectrometer. The problem with such an experiment in systems such as CO on transition metals, is that the non-radiative relaxation rates are apparently many orders of magnitude faster than the radiative rate, with the result that the efficiency of the luminescence process is prohibitively small. The small probability of radiative decay does not affect the equilibrium experiment--the principle of detailed balance ensures that the decay and excitation rates for all of the non-radiative processes are equal--but it makes the measurement of non-equilibrium radiation very difficult. Systems with molecules on insulating substrates with vibrational frequencies much larger than substrate phonon frequencies, such as those studied by Chuang[72] are more promising. In such a case, the non-radiative decay processes can

be slow enough to make the luminescence experiment feasible. Other strategies could include the use of cooled samples or samples with very high surface areas, such as dispersed catalysts.

Acknowledgments

We are grateful to P. Dumas for help in characterizing the bolometric sample, and for permission to quote direct absorption results before publication. Thanks are also due to E. E. Haller and his group for providing some of the thermometer chips used in the direct absorption experiment.

Our co-workers, R. B. Bailey and S. Chiang had a major role in the development of the direct absorption and emission techniques, respectively.

This work was supported by the Director, Office of Energy Research, Office of Basic Energy Sciences, Materials Sciences Division of the U.S. Department of Energy under Contract No. DE-AC03-76SF00098.

REFERENCES

1. F. M. Hoffmann, Infrared reflection-absorption spectroscopy of adsorbed molecules, Surf. Sci. Rep. 3, 107-192 (1983).

2. R. Ryberg, Infrared spectroscopy of adsorbed molecules: some experimental aspects, J. Phys. Colloque 44, CIO-421-426 (1983).

3. R. G. Greenler, Reflection method for obtaining the infrared spectrum of a thin layer on a metal surface, J. Chem. Phys. 50, 1963-1968 (1969).

4. J. F. Blanke and J. Overend, Infrared spectroscopy of surface species; emission spectra from a semi-blackbody, Spectrochim. Acta 32A, 1383-1386 (1976).

5. Y. J. Chabal, Hydrogen vibration on Si(111)7 × 7: evidence for a unique chemisorption site, Phys. Rev. Lett. 50, 1850-1853 (1983).

6. Y. J. Chabal and A. J. Sievers, High-resolution infrared study of hydrogen (1 × 1) on tungsten (100), Phys. Rev. Lett. 44, 944-947 (1980).

7. D. K. Lambert, Observation of the first order Stark effect of CO on Ni(110), Phys. Rev. Lett. 50, 2106-2109 (1983).

8. F. M. Hoffmann and A. M. Bradshaw, Infrared spectroscopy of CO adsorbed on palladium (100) and (111) surfaces, in: Proceedings Third International Conference on Solid Surfaces, (Vienna, 1977), pp. 1167-1170.

9. W. G. Golden, D. S. Dunn, and J. Overend, A method for measuring infrared reflection-absorption spectra of molecules adsorbed on low-area surfaces at monolayer and submonolayer concentrations, J. Catalysis 71, 395-404 (1981).

10. R. Ryberg, Carbon monoxide adsorbed on Cu(100) studied by infrared spectroscopy, Surf. Sci. 114, 627-641 (1982), and references therein.

11. D. P. Woodruff, B. E. Hayden, K. Prince, and A. M. Bradshaw, Dipole coupling and chemical shifts in IRAS of CO adsorbed on Cu(110), Surf. Sci. 123, 397-412 (1982).

12. W. G. Golden, D. D. Saperstein, M. W. Severson, and J. Overend, Infrared reflection-absorption spectroscopy of surface species: a comparison of Fourier transform and dispersion methods, J. Phys. Chem. 88, 574-580 (1984).

13. W. B. Jackson, N. M. Amer, A. C. Boccara, and D. Fournier, Photothermal deflection spectroscopy and detection, Appl. Opt. 20, 1333-1344 (1981).

14. C. K. N. Patel and A. C. Tam, Pulsed photoacoustic spectroscopy of condensed matter, Rev. Mod. Phys. 53, 517-550 (1981).

15. A. Otto in: Light Scattering in Solids, Vol. 4, (M. Cardona and G. Guntherolt, eds.), Vol. 4, pp. 289-418, Springer, Berlin (1984), and references therein.

16. Y. R. Shen, in: Novel Materials and Techniques in Condensed Matter, (G. W. Crabtree and P. Vashishta, eds.), pp. 193-208, Elsevier (1982), and references therein.

17. A. Mooradian, Tunable infrared lasers, Rep. Prog. Phys. 42, 1533-1564 (1979).

18. C. K. N. Patel, The Free Electron Laser, National Academy Press, Washington, D.C. (1982).

19. S. Silver, Microwave antenna theory and design, pp. 50-51, McGraw Hill, New York (1949).

20. Kwang-Je Kim, private communication.

21. W. D. Duncan and G. P. Williams, Infrared synchrotron radiation from electron storage rings, Appl. Opt. 22, 2914-2923 (1983).

22. E. H. Putley, Solid state devices for infra-red detection, J. Sci. Instrum. 43, 857-868 (1966).

23. M. R. Hueschen, P. L. Richards, and E. E. Haller, Performance of Ge:Ga far infrared detectors, Proceedings of the NASA Infrared Detector Technology Workshop (August 1983), p. 3-1.

24. E. L. Dereniak, R. R. Joyce, and R. W. Capps, Low noise preamplifier for photoconductive detectors, Rev. Sci. Instrum. 48, 392-394 (1977).

25. F. J. Low, Integrating amplifiers using cooled JFETS, Appl. Opt. 23, 1309-1310 (1984).

26. P. L. Richards and L. T. Greenberg, in: Infrared and Millimeter Waves, (K. J. Button, ed.), Vol. 6, pp. 149-207, Academic Press, New York (1982).

27. N. S. Nishioka, P. L. Richards, and D. P. Woody, Composite bolometers for submillimeter wavelengths, Appl. Opt. 17, 1562-1567 (1978).

28. A. E. Lange, E. Kreysa, S. E. McBride, and P. L. Richards, Improved fabrication techniques for infrared bolometers, Int. J. of Infrared and Millimeter Waves 4, 689-706 (1983).

29. R. J. Bell, Introductory Fourier Transform Spectroscopy, Academic Press, New York (1972).

30. N. P. Palaio, M. Rodder, E. E. Haller, and E. Kreysa, Neutron transmutation-doped germanium bolometers, Int. J. of Infrared and Millimeter Waves 4, 933-943 (1983).

31. F. J. Low and A. R. Hoffman, The detectivity of cryogenic bolometers, Appl. Opt. 2, 649-650 (1963).

32. C. Kittel and H. Kroemer, Thermal Physics, W. H. Freeman, San Francisco (1980).

33. R. B. Bailey, T. Iri, and P. L. Richards, Infrared spectra of carbon monoxide on evaporated nickel films: a low temperature thermal detection technique, Surf. Sci. 180, 626-646 (1980).

34. J. C. Burgiel and L. C. Hebel, Far infrared spin and combination resonance in bismuth, Phys. Rev. 140, A925-A929 (1965).

35. H. E. Grenga, K. R. Lawless, and L. B. Garmon, Structure and topography of monocrystalline nickel thin films grown by vapor deposition, J. Appl. Phys. 42, 3629-3633 (1971).

36. J. Kleefeld, B. Pratt, and A. A. Hirsch, Epitaxial growth of nickel from the vapour phase, J. Crystal. Growth 19, 141-146 (1973).

37. Stycast 2850 GT, Emerson and Cuming Co., Canton, Massachusetts.

38. P. Dumas, R. G. Tobin, and P. L. Richards, Study of adsorption states and interactions of CO on evaporated noble metal surfaces by infrared absorption spectroscopy, I. Silver, to be published.

39. P. Dumas, R. G. Tobin, and P. L. Richards, Study of adsorption states and interactions of CO on evaporated noble metal surfaces by infrared absorption spectroscopy, II. Gold and copper, to be published.

40. S. Klause, C. Mariani, K. C. Prince, and K. Horn, Screening effects in photoemission from weakly bound adsorbates: CO on Ag(110), Surf. Sci. 138, 305-318 (1984).

41. A. Crossley and D. A. King, Adsorbate island dimensions and interaction energies from vibrational spectra: CO on Pt{001} and Pt{111}, Surf. Sci. 95, 131-155 (1980).

42. A. Crossley and D. A. King, Infrared spectra for CO isotopes chemisorbed on Pt{111}: evidence for strong adsorbate coupling interactions, Surf. Sci. 68, 528-538 (1977).

43. R. M. Hammaker, S. A. Francis, and R. P. Eischens, Infrared study of intermolecular interactions for carbon monoxide chemisorbed on platinum, Spectrochim. Acta 21, 1295-1309 (1965).

44. B. N. J. Persson and R. Ryberg, Vibrational interaction between molecules adsorbed on a metal surface: The dipole-dipole interaction, Phys. Rev. B24, 6954-6970 (1981).

45. M. Moskovits and J. E. Hulse, Frequency shifts in the spectra of molecules adsorbed on metals, with emphasis on the infrared spectrum of adsorbed CO, Surf. Sci. 78, 397-418 (1978).

46. P. Geraghty, M. Wixom, and A. H. Francis, Photocalorimetric spectroscopy and ac calorimetry of thin surface films, J. Appl. Phys. 55, 2780-2785 (1984).

47. S. Chiang, R. G. Tobin, and P. L. Richards, Vibrational spectroscopy of chemisorbed molecules by infrared emission, J. Vac. Sci. and Technol. A2, 1069-1074 (1984).

48. P. R. Griffiths, Chemical Infrared Fourier Transform Spectroscopy, John Wiley & Sons, New York (1975).

49. D. Kember and N. Sheppard, The use of ratio-recording interferometry for the measurement of infrared emission spectra: applications to oxide films on copper surfaces, Appl. Spectrosc. 29, 496-500 (1975).

50. L. M. Gratton, S. Paglia, F. Scattaglia, and M. Cavallini, Infrared emission spectroscopy applied to the oxidation of molybdenum, Appl. Spectrosc. 32, 310-316 (1978).

51. M. Adachi, K. Kishi, T. Imanaka, and S. Teranishi, Infrared emission spectra of formic acid adsorbed on V_2O_5, Bull. Chem. Soc. Japan 40, 1290-1292 (1967).

52. O. Koga, T. Onishi, and K. Tamaru, Infrared emission spectra of formic acid adsorbed on alumina, J. Chem. Soc., Chem. Comm., 464 (1974).

53. M. Primet, P. Fouilloux, and B. Imelik, Propene-V_2O_5 interactions studied by infrared emission spectroscopy, Surf. Sci. 85, 457-470 (1979).

54. M. Primet, P. Fouilloux, and B. Imelik, Chemisorptive properties of platinum supported on zeolite Y studied by infrared emission spectroscopy, J. Catalysis 61, 553-558 (1980).

55. D. L. Allara, D. Teicher, and J. F. Durana, Fourier transform infrared emission spectrum of a molecular monolayer at 300 K, Chem. Phys. Lett. 84, 20-24 (1981).

56. JFET 00, Infrared Laboratories, Inc., Tucson, AZ.

57. L. Harris and J. K. Beasley, The infrared properties of gold smoke deposits, J. Opt. Soc. Am. 42, 134-140 (1952).

58. L. Harris, The transmittance and reflectance of gold black deposits in the 15- to 100-micron region, J. Opt. Soc. Am. 51, 80-82 (1961).

59. L-51 Taut band chopper, Bulova Watch Co., Woodside, N.Y.

60. H. Ibach, Comparison of cross sections in high resolution electron energy loss spectroscopy and infrared reflection spectroscopy, Surf. Sci. 66, 56-66 (1977).

61. R. G. Tobin, S. Chiang, P. A. Thiel, and P. L. Richards, The C=O stretching vibration of CO on Ni(100) by infrared emission spectroscopy, Surf. Sci. 140, 393-399 (1984).

62. S. Chiang, R. G. Tobin, P. L. Richards, and P. A. Thiel, The molecule-substrate vibration of CO on Ni(100) studied by infrared emission spectroscopy, Phys. Rev. Lett. 52, 648-651 (1984).

63. R. G. Tobin and P. L. Richards, to be published.

64. J. C. Ariyasu, D. L. Mills, K. G. Lloyd, and J. C. Hemminger, Anharmonic damping of adsorbate vibrational modes, Phys. Rev. B28, 6123-6126 (1984).

65. M. J. Dignam in: Vibrations at Surfaces: Proceedings of an International Conference at Namur, Belgium, (R. Caudano, J. M. Gilles, and A. A. Lucas, eds.), pp. 265-288, Plenum Press, New York (1982).

66. J. C. Tracy, Structural influences on adsorption energy. II. CO on Ni(100), J. Chem. Phys. 56, 2736-2747 (1972).

67. G. E. Mitchell, J. L. Gland, and J. M. White, Vibrational spectra of coadsorbed CO and H on Ni(100), Surf. Sci. 131, 167-178 (1983).

68. S. Andersson, Vibrational excitations and structure of CO adsorbed on Ni(100), Solid State Commun. 21, 75-81 (1977).

69. J. C. Bertolini and B. Tardy, Vibrational EELS studies of CO chemisorption on clean and carbided (111), (100), and (110) nickel surfaces, Surf. Sci. 102, 131-150 (1981).

70. C. R. McCreight, Two-dimensional infrared detector arrays, Proc. IAU Colloq. 79, 585-602 (1984).

71. D. M. Rank, Astronomical applications of IR CID technology, final report, NASA CR 166-584 (1984).

72. T. J. Chuang, Infrared chemiluminescence from XeF_2-silicon-surface reactions, Phys. Rev. Lett. 42, 815-817 (1979).

FIGURE CAPTIONS

Figure 1(a) Absorptance of a cold Ni surface as a function of angle of incidence and direction of polarization.

(b) Ratio of the peak absorptance of the C-O stretch vibration of chemisorbed CO to the absorptance and the reflectance of a cold Ni surface.

Figure 2. Infrared power per mode as a function of photon frequency for thermal sources at 1200 and 2000°K compared with the time averaged power computed from a bending magnet and a wiggler magnet on a proposed synchrotron light source. The power per mode is given in temperature units defined in the text.

Figure 3. Measurements of noise equivalent photon rate NEN versus photon rate N for a Ge:Ga detector at 100 cm^{-1} (100 μm). The data agree with the photon noise computed from Eq.(1) with $\eta = 1$ to the experimental uncertainty, which is a factor ~3 in N.

Figure 4. Vertical cross section of cryostat and sample chamber for direct absorption experiment.

Figure 5. Sample assembly for direct absorption experiment on evaporated films.

Figure 6. Infrared spectrum of 10^{-3} L CO chemisorbed at 2°K on a silver film deposited at T_D = 4°K, showing a single band at 2148 cm^{-1}. The integration time was ~40 min. The spectrometer resolution was 8 cm^{-1}.

Figure 7. Infrared spectra of CO physisorbed at 2°K on a silver film deposited at T_D = 300°K, as a function of exposure in Langmuir showing a single narrow band at 2143 cm^{-1}. The spectrometer resolution was 4 cm^{-1}.

Figure 8. Infrared spectra of CO chemisorbed at 2°K on a silver film deposited at T_D = 4°K. A broad band due to chemisorbed CO appears at low coverage at 2148 cm^{-1}, and shifts to lower frequency with increasing exposure. At 0.4 L, a sharp band due to physisorbed CO appears at 2143 cm^{-1}, and the band due to chemisorbed CO shifts further to low frequency. The spectrometer resolution was 4 cm^{-1}.

Figure 9. Total frequency shift of the CO stretch vibration from Fig. 8, and chemical shift deduced from isotopic substitution as a function of exposure. The lines are drawn as a guide for the eye.

Figure 10 (a) Dynamic contribution to the frequency shift, derived from data in Fig. 9, for chemisorbed CO on a silver film, T_D = 4°K.

(b) Integrated band intensity, from Fig. 4. The lines are theoretical fits to the data, using the Persson-Ryberg dipole coupling model with $\alpha_v = 0.27$ $Å^3$ and $\tilde{U}(0) = 0.04$ $Å^{-3}$.

Figure 11. Optical layout of infrared emission apparatus, with LHe-cooled spectrometer on the left and ultrahigh vacuum system on the right.

Figure 12. The solid curves show the calculated detection threshold for our emission apparatus if it were limited by photon noise. The dashed lines show the experimental sensitivity without modulation. The x's show the measured surface signal from CO on Ni(100). The dots and chemical symbols indicate the signal levels to be expected from monolayer coverages of various adsorbates on Pt(111).

Figure 13. IR emission spectra of CO on a clean Ni(100) surface at 310°K. The instrumental resolution was ~18 cm^{-1}.

Figure 14. Infrared emission spectra from a saturation coverage of CO on Ni(100) at 310°K. The instrumental resolution was 2.5 cm^{-1}, and a linear baseline has been subtracted from the curves. The solid lines are obtained by computer smoothing of the data.

(a) Spectrum of a disordered CO layer on a partially contaminated surface.

(b) Spectrum of an ordered c(2×2) CO overlayer on a clean surface.

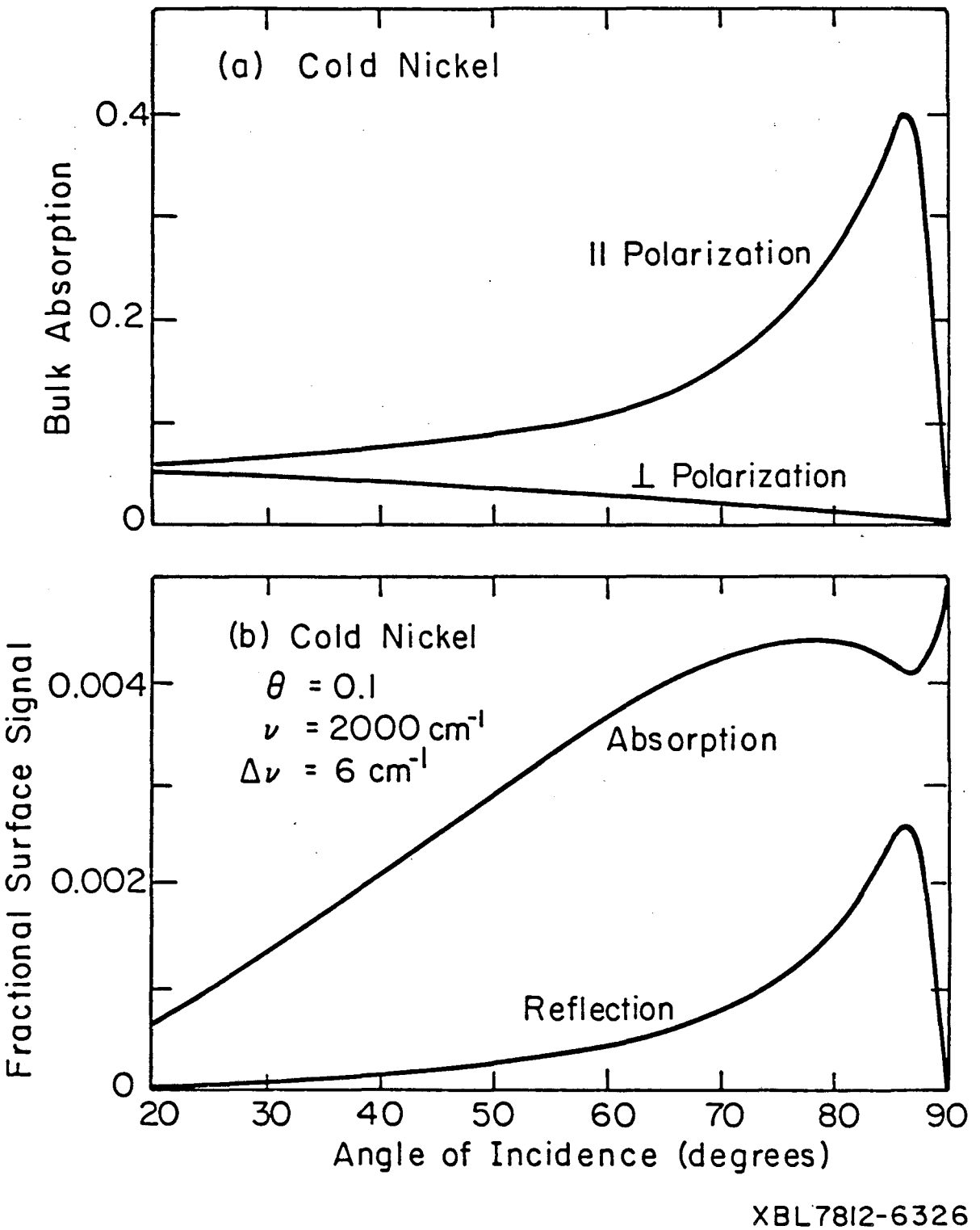
(a) Cold Nickel
Bulk Absorption
0.4
0.2
0
II Polarization
⊥ Polarization
(b) Cold Nickel
θ = 0.1
ν = 2000 cm⁻¹
Δν = 6 cm⁻¹
Fractional Surface Signal
0.004
0.002
0
Absorption
Reflection
20
30
40
50
60
70
80
90
Angle of Incidence (degrees)
XBL7812-6326

FIGURE 1

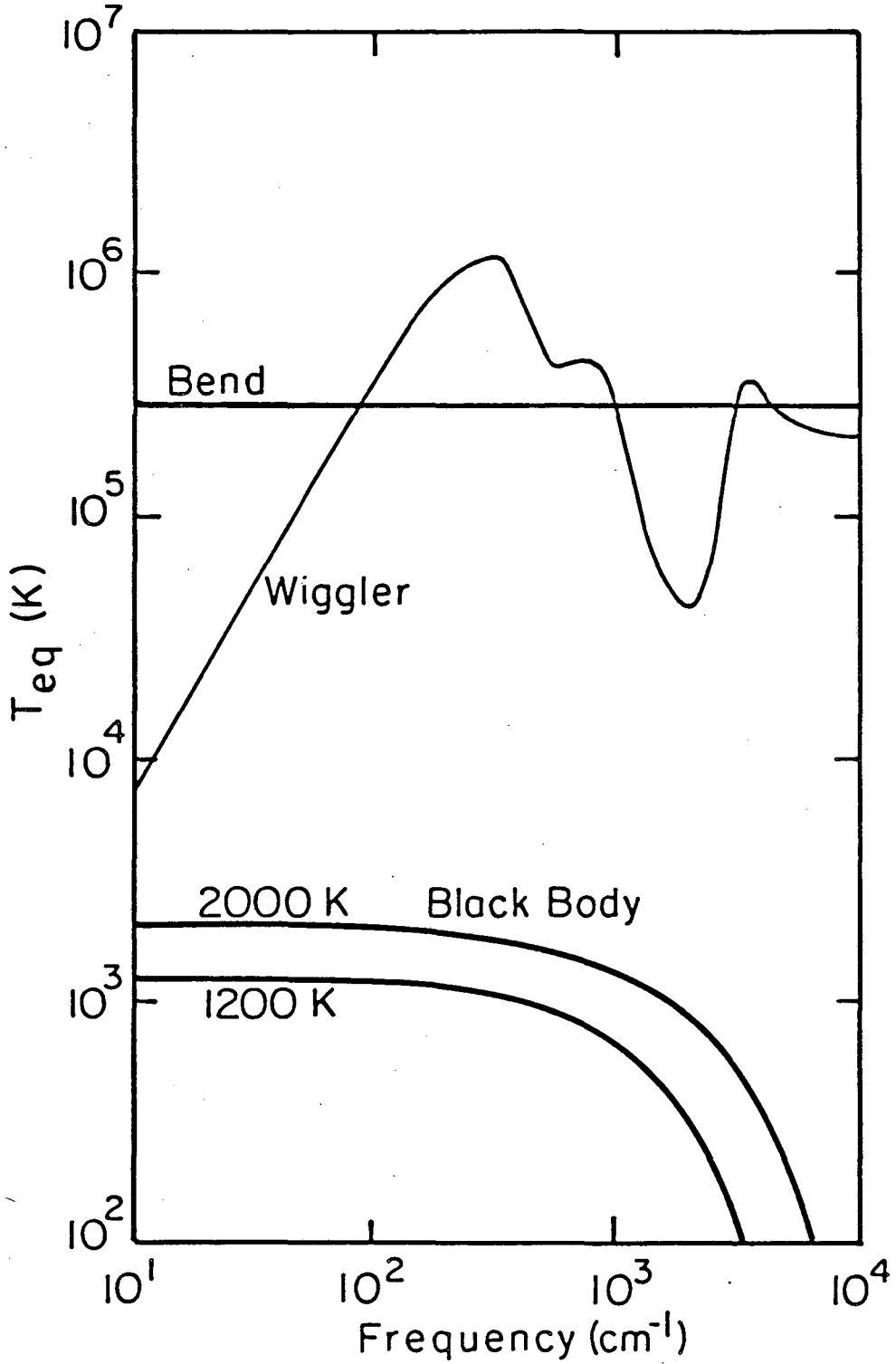
10^7
10^6
10^5
10^4
10^3
10^2
Bend
Wiggler
T_{eq} (K)
2000 K
Black Body
1200 K
10^1
10^2
10^3
10^4
Frequency (cm^{-1})
XBL 831-14A

FIGURE 2

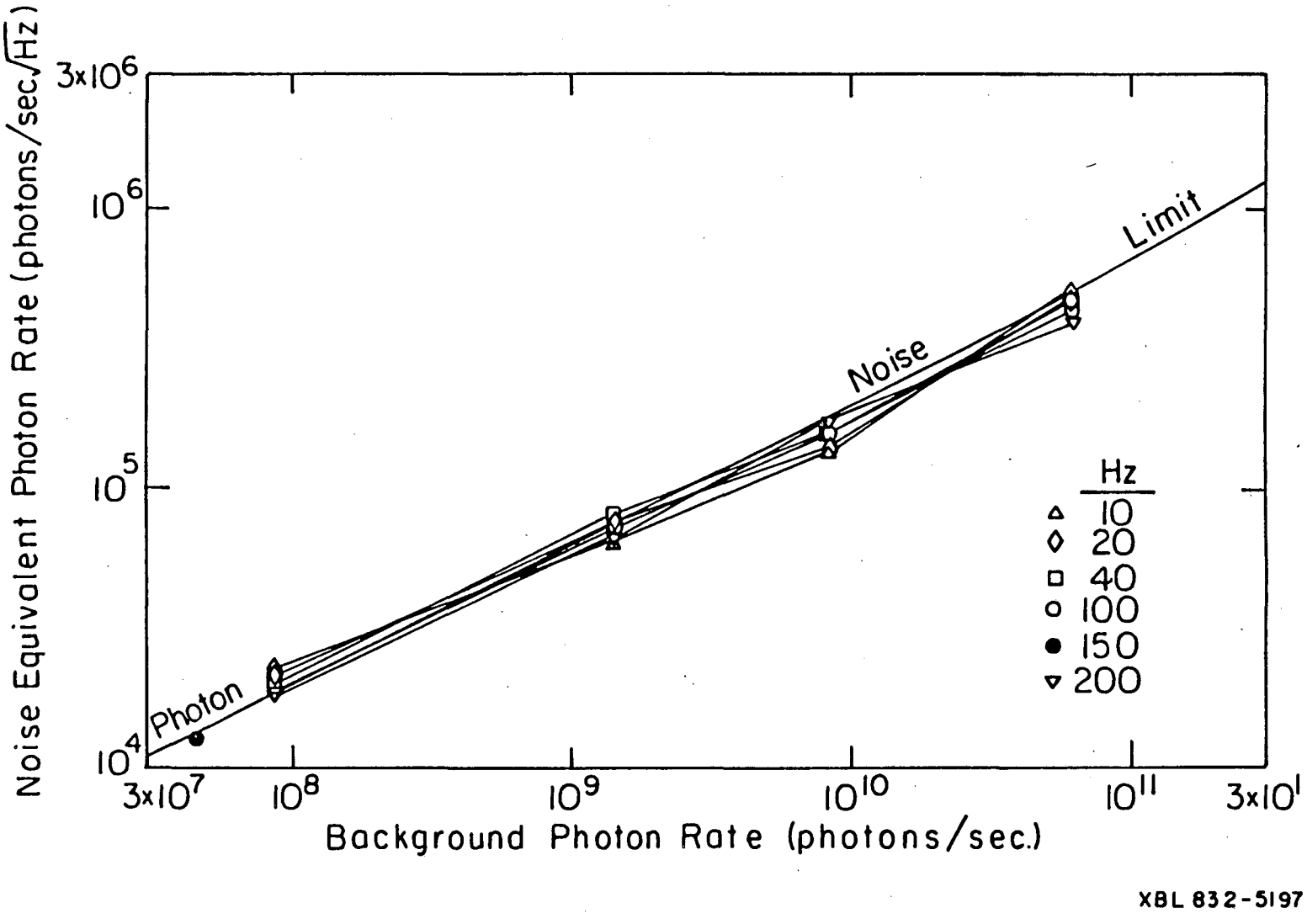
Noise Equivalent Photon Rate (photons/sec/√Hz)
3x10^6
10^6
10^5
10^4
Photon
Noise
Limit
Hz
10
20
40
100
150
200
3x10^7
10^8
10^9
10^10
10^11
3x10^11
Background Photon Rate (photons/sec.)
XBL 832-5197

FIGURE 3

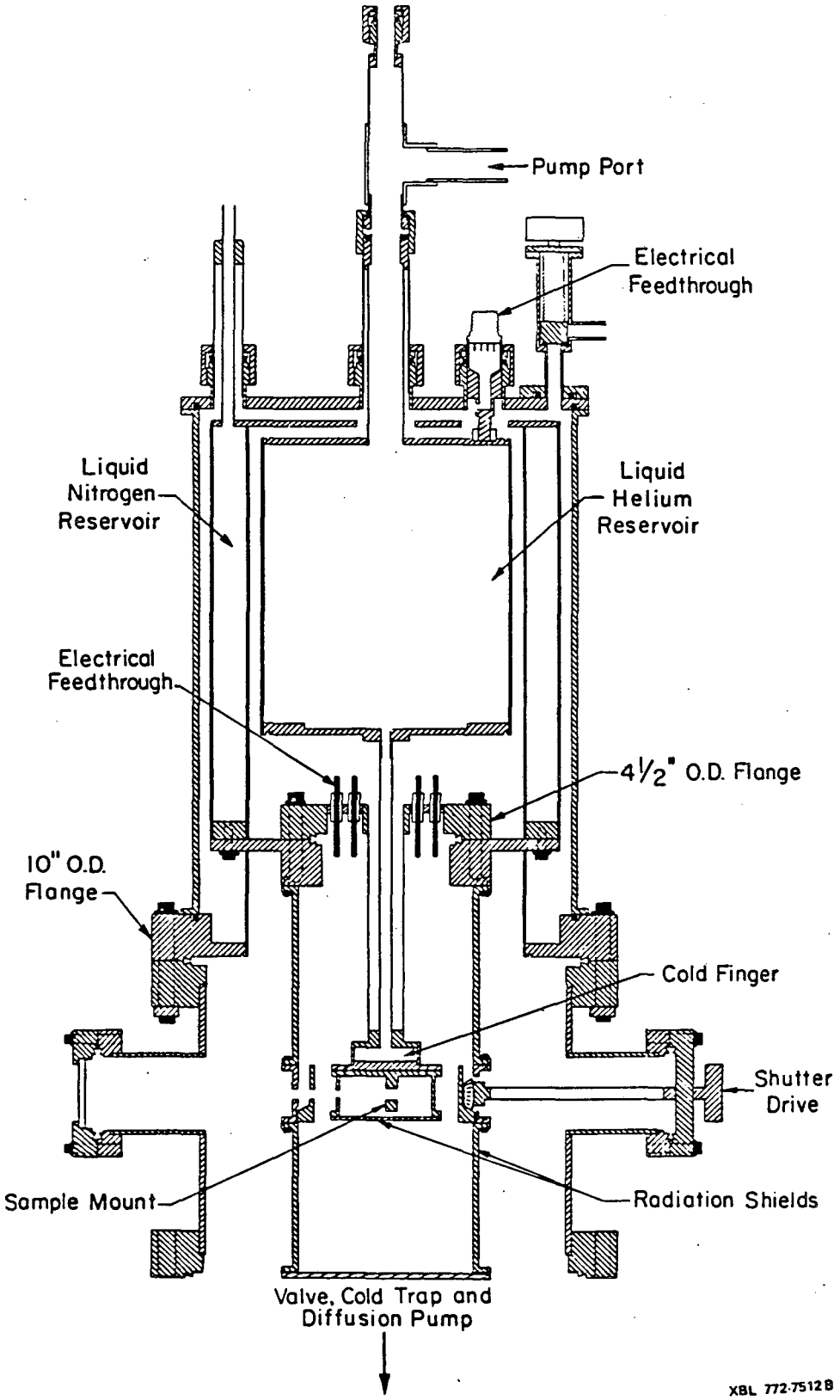
Pump Port
Electrical Feedthrough
Liquid Nitrogen Reservoir
Liquid Helium Reservoir
Electrical Feedthrough
4½" O.D. Flange
10" O.D. Flange
Cold Finger
Shutter Drive
Sample Mount
Radiation Shields
Valve, Cold Trap and Diffusion Pump
XBL 772-7512B

FIGURE 4

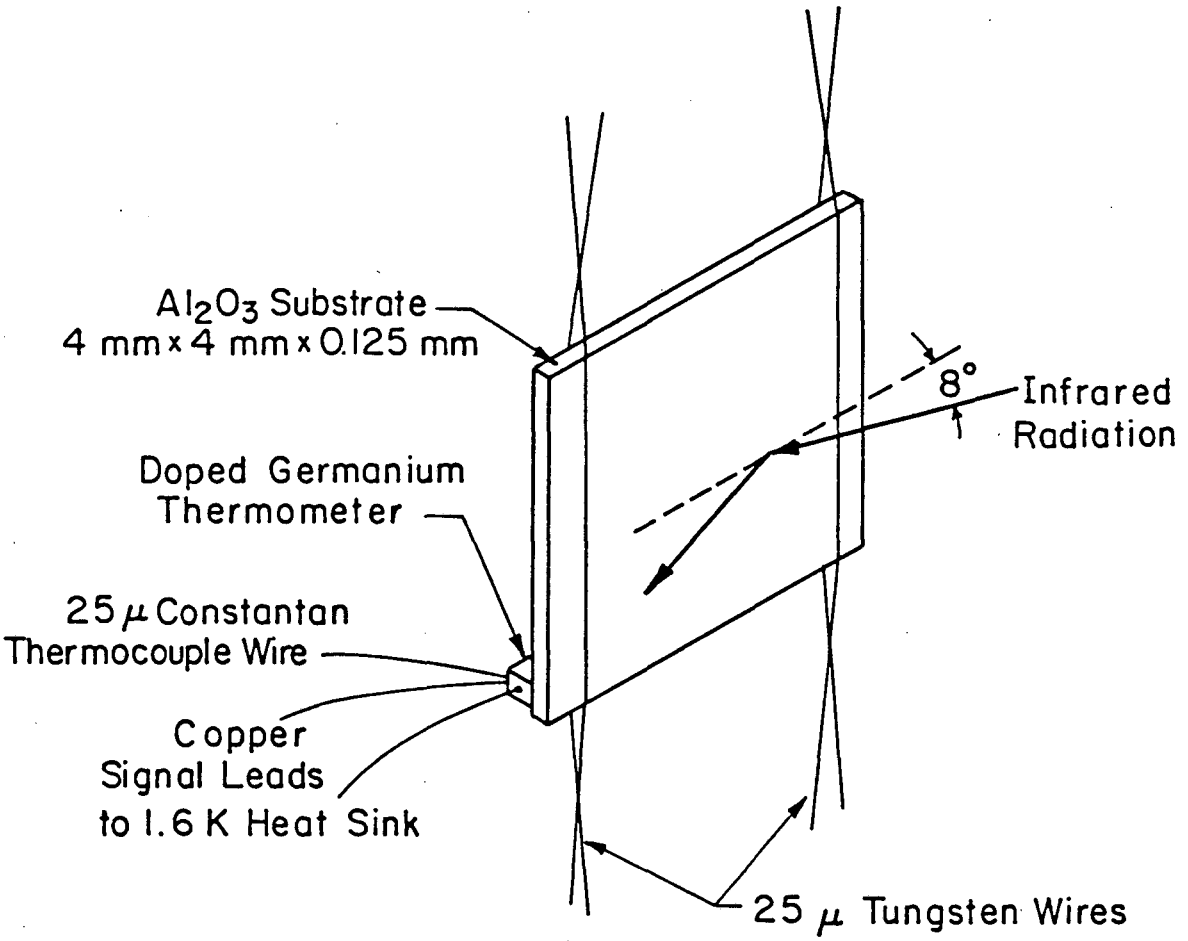
Al_2O_3 Substrate
4 mm x 4 mm x 0.125 mm
Doped Germanium
Thermometer
25 μ Constantan
Thermocouple Wire
Copper
Signal Leads
to 1.6 K Heat Sink
8°
Infrared
Radiation
25 μ Tungsten Wires
XBL 786-5118A

FIGURE 5

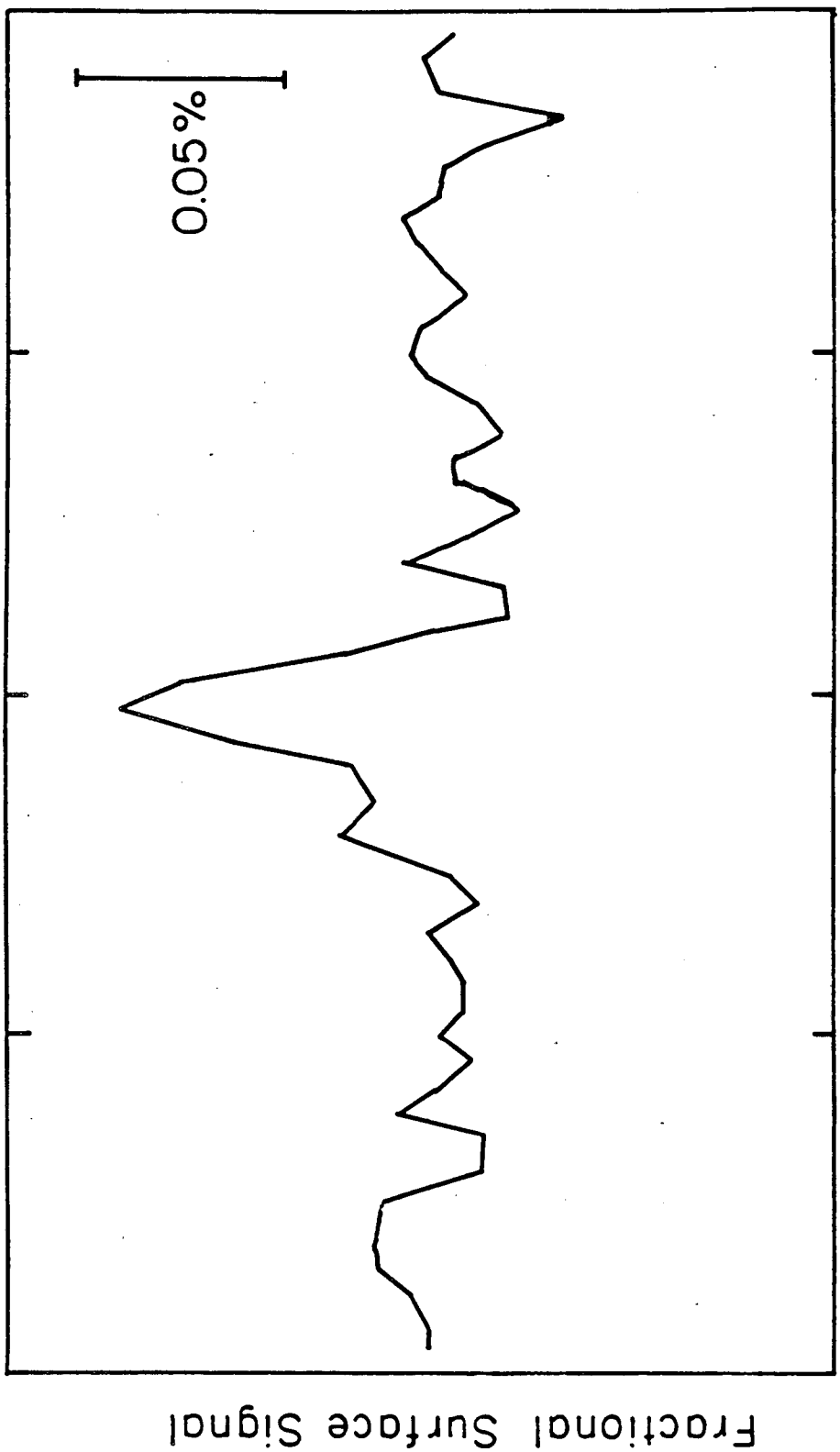
Fractional Surface Signal
0.05%
2100
2150
2200
Wavenumber (cm⁻¹)
XBL854-6053

FIGURE 6

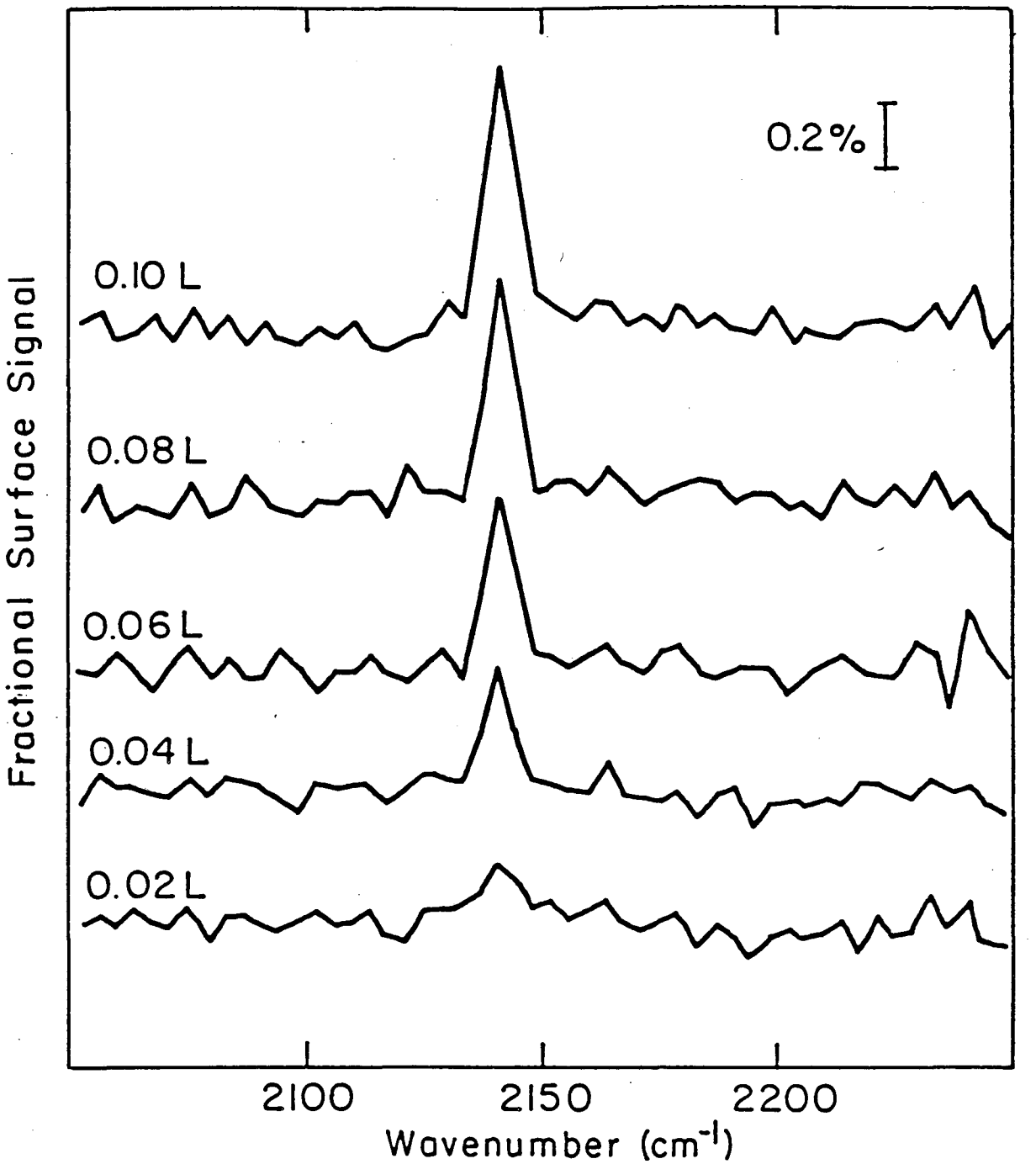

XBL 854-6055

FIGURE 7

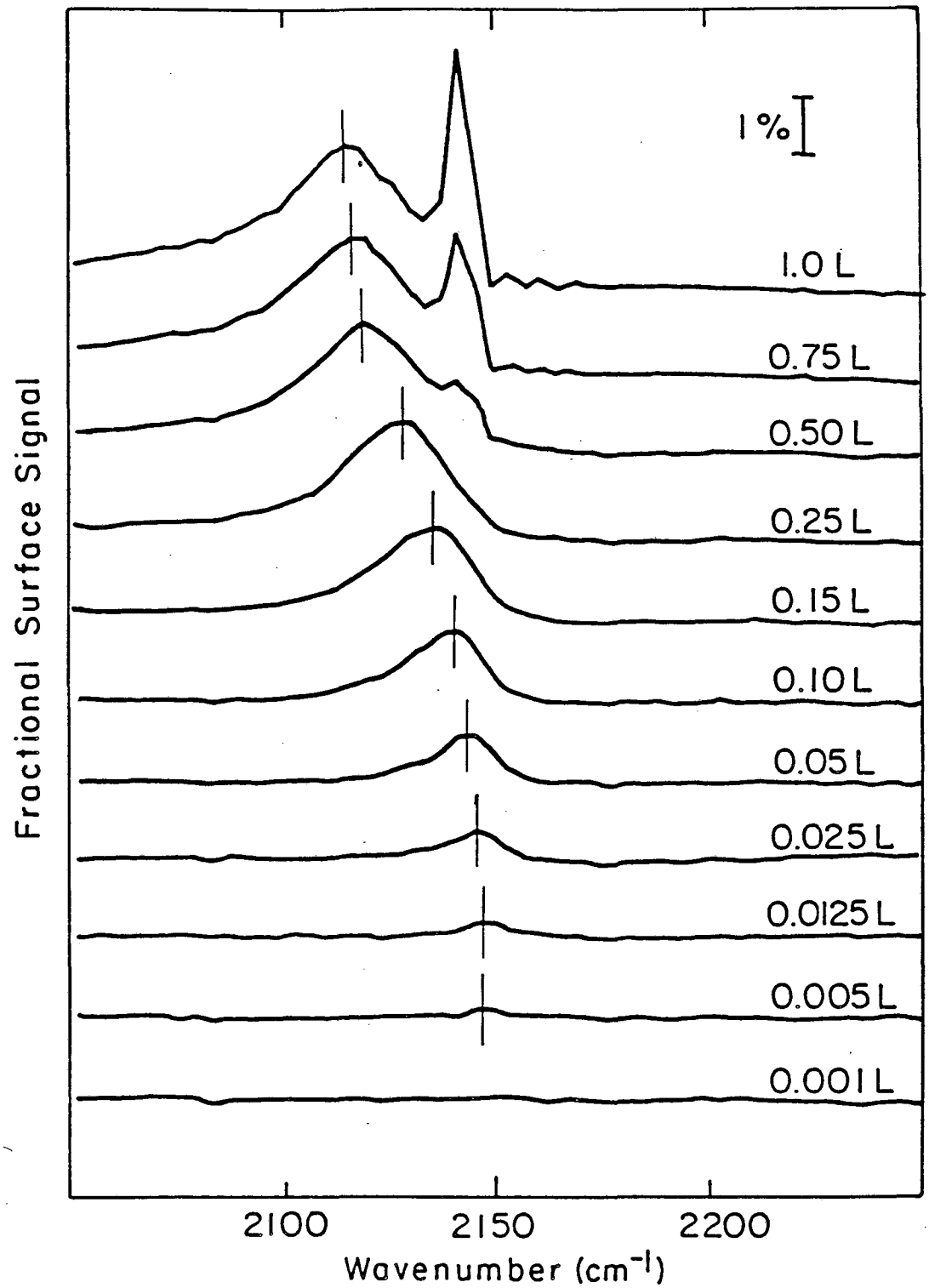
1%
1.0 L
0.75 L
0.50 L
0.25 L
0.15 L
0.10 L
0.05 L
0.025 L
0.0125 L
0.005 L
0.001 L
Fractional Surface Signal
2100
2150
2200
Wavenumber (cm⁻¹)
XBL 854-6052

FIGURE 8

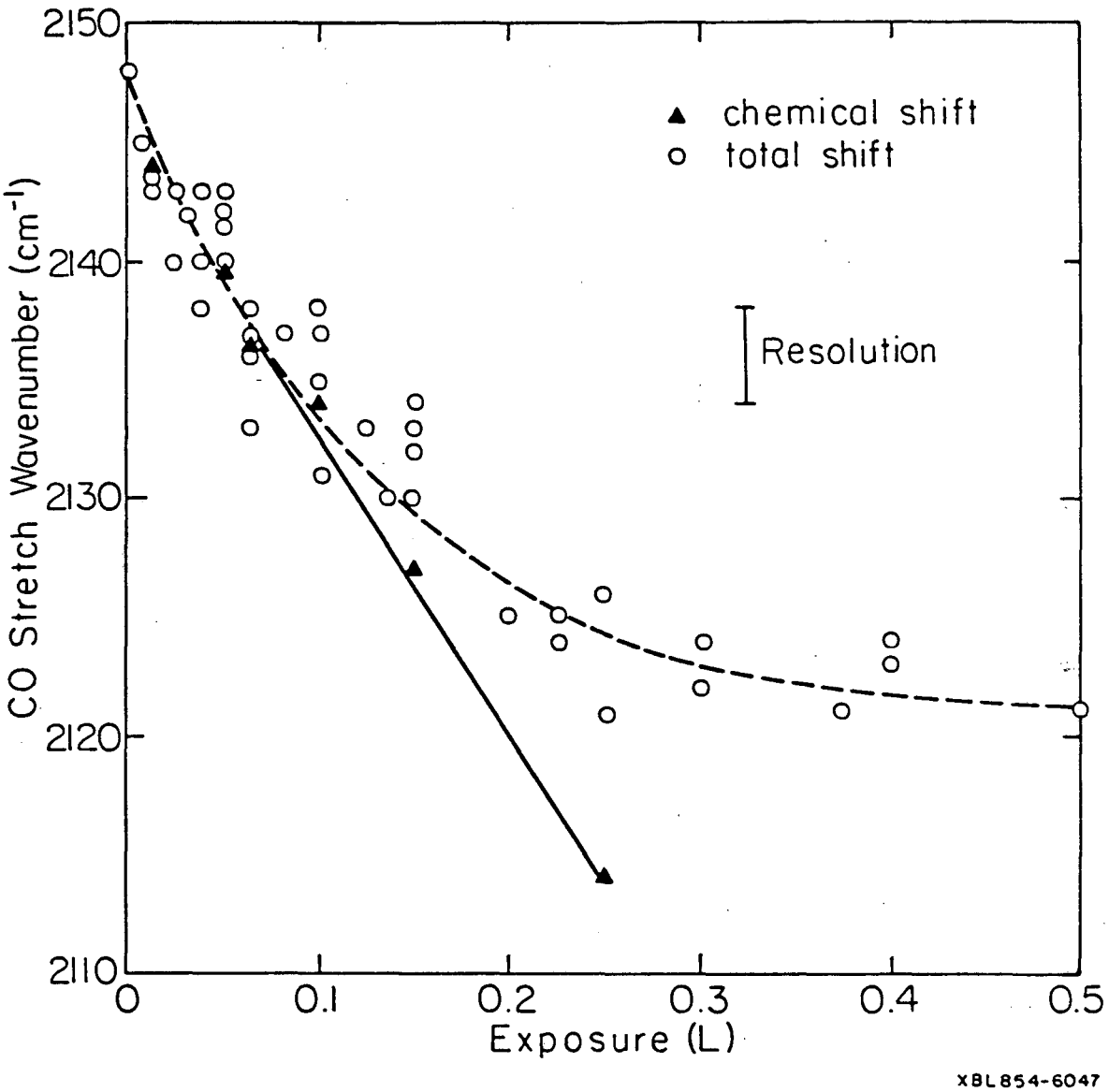
2150
2140
2130
2120
2110
CO Stretch Wavenumber (cm⁻¹)
0
0.1
0.2
0.3
0.4
0.5
Exposure (L)
▲ chemical shift
o total shift
Resolution
XBL854-6047

FIGURE 9

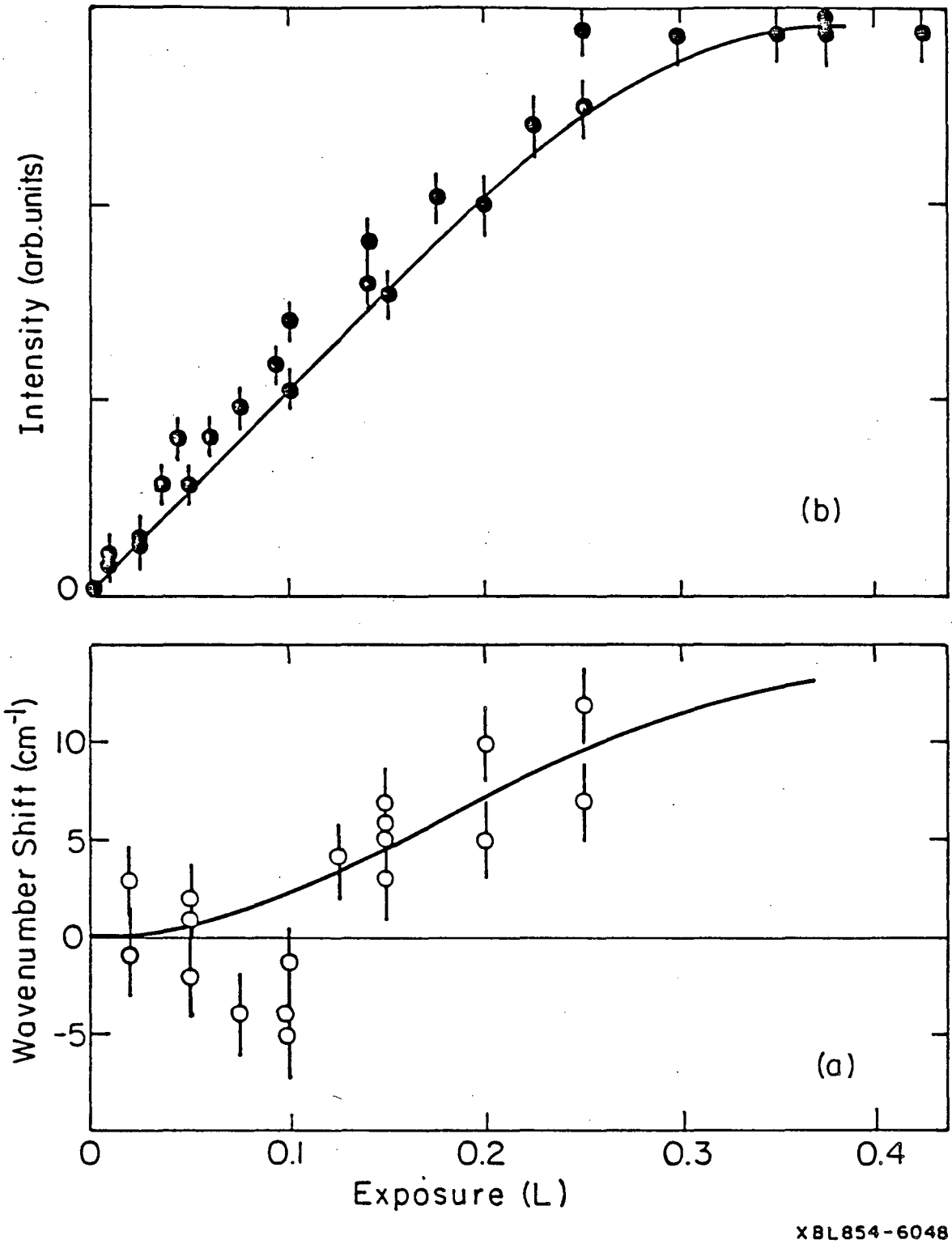
Intensity (arb.units)
0
(b)
Wavenumber Shift (cm⁻¹)
10
5
0
-5
(a)
0
0.1
0.2
0.3
0.4
Exposure (L)
XBL854-6048

FIGURE 10

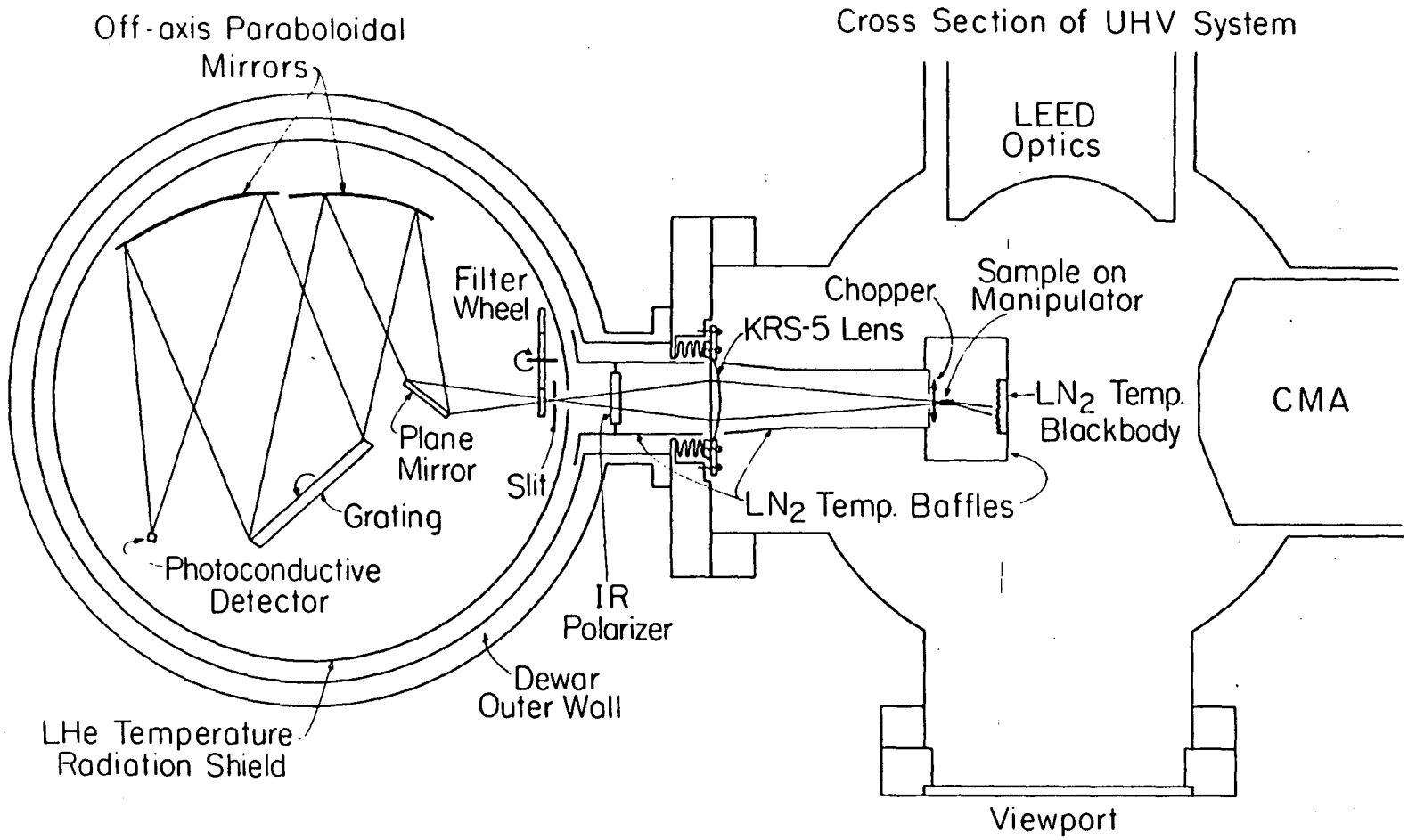

Optical Layout of Infrared Emission Spectrometer

XBL 8012-13382 B

FIGURE 11

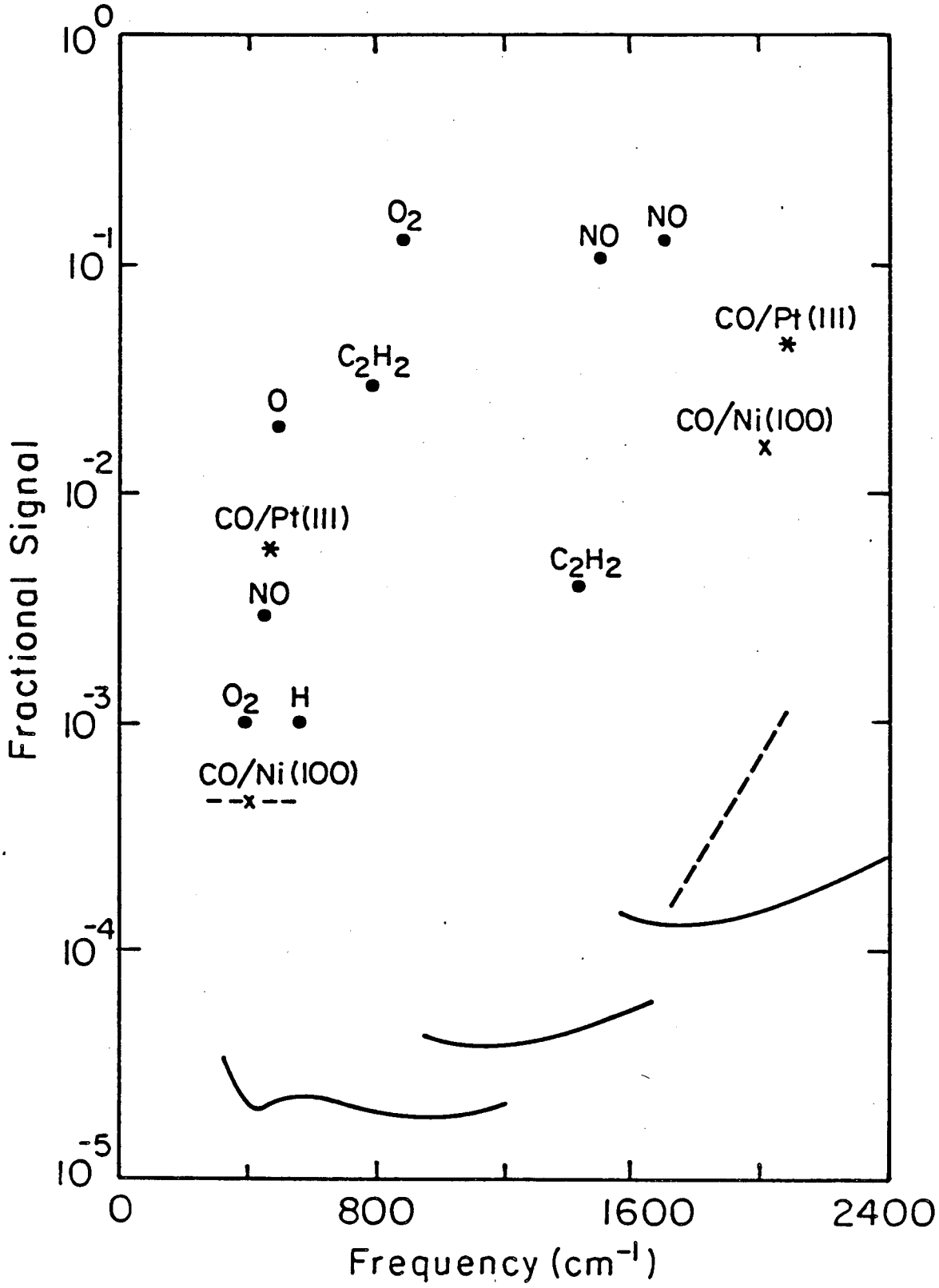
Fractional Signal
10^{0}
10^{-1}
10^{-2}
10^{-3}
10^{-4}
10^{-5}
O_2
NO
NO
CO/Pt(111)
C_2H_2
O
CO/Ni(100)
CO/Pt(111)
C_2H_2
NO
O_2
H
CO/Ni(100)
0
800
1600
2400
Frequency (cm^{-1})
XBL 838-11018A

FIGURE 12

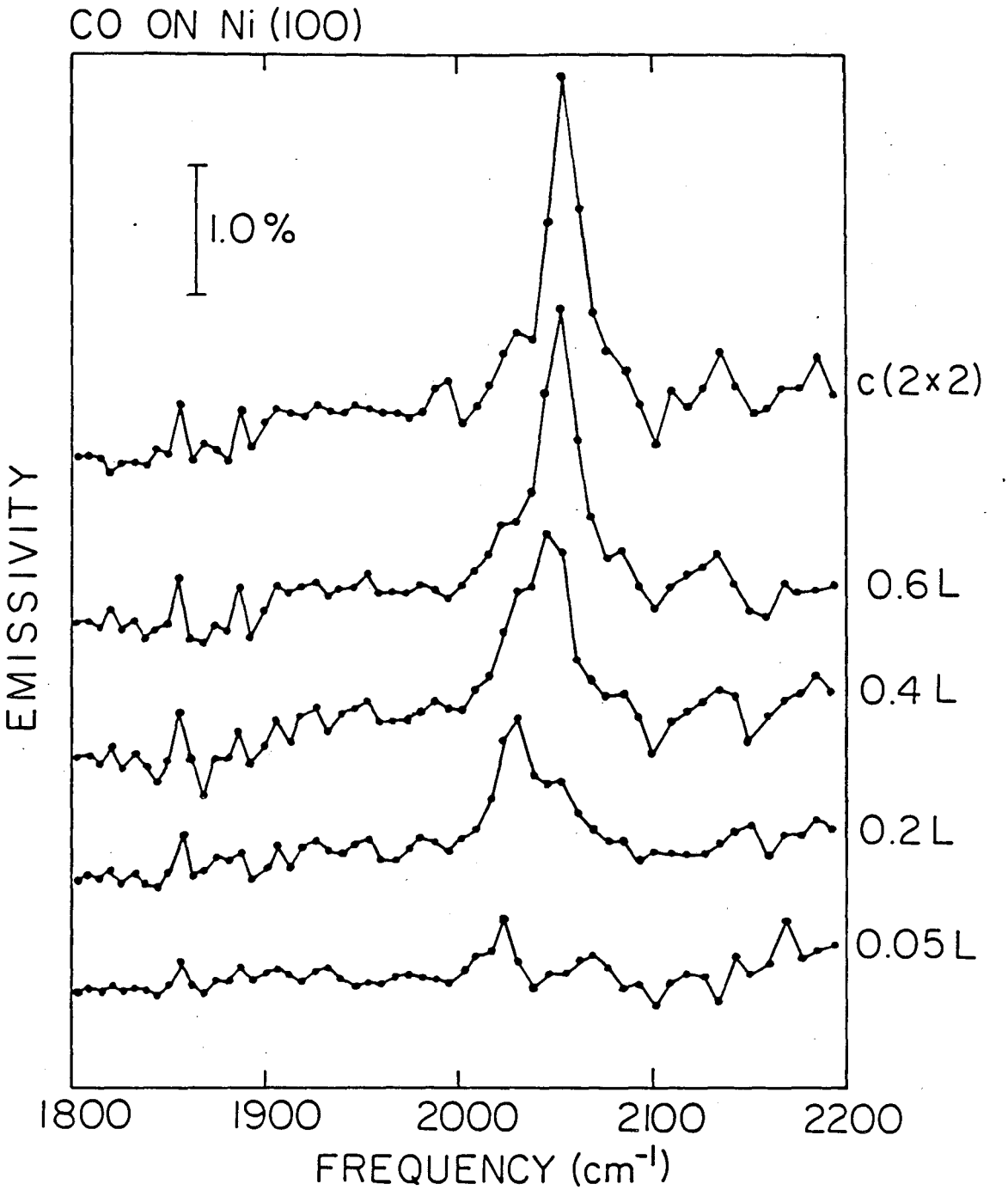
CO ON Ni (100)
1.0%
c(2x2)
0.6L
0.4L
0.2L
0.05L
EMISSIVITY
1800
1900
2000
2100
2200
FREQUENCY (cm⁻¹)
XBL839-6426

FIGURE 13

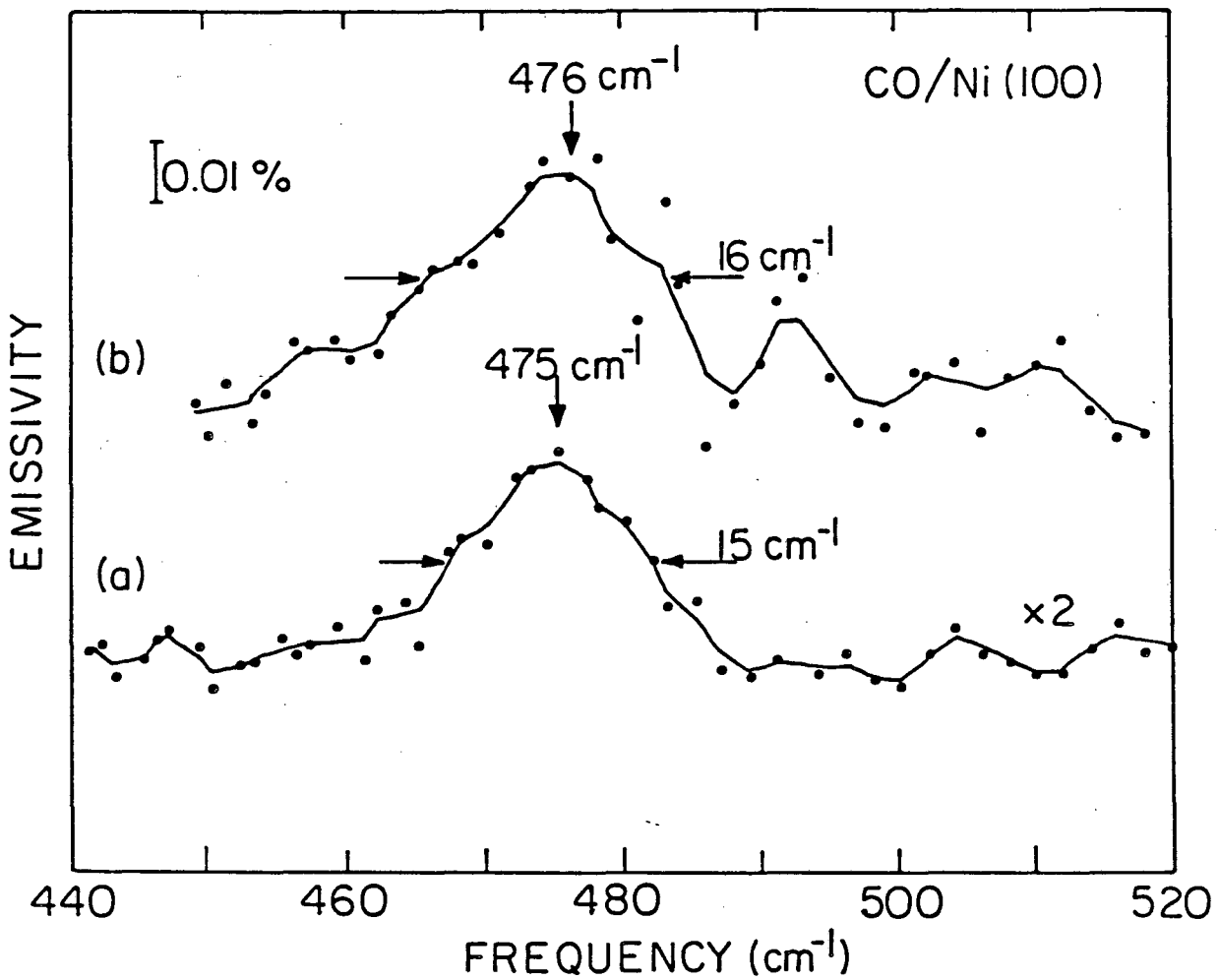
476 cm⁻¹
CO/Ni (100)
0.01 %
16 cm⁻¹
(b)
475 cm⁻¹
15 cm⁻¹
(a)
x2
EMISSIVITY
440
460
480
500
520
FREQUENCY (cm⁻¹)
XBL8311-6595

FIGURE 14

LAWRENCE BERKELEY LABORATORY
TECHNICAL INFORMATION DEPARTMENT
UNIVERSITY OF CALIFORNIA
BERKELEY, CALIFORNIA 94720